

Dear Author

Please use this PDF proof to check the layout of your article. If you would like any changes to be made to the layout, you can leave instructions in the online proofing interface. First, return to the online proofing interface by clicking "Edit" at the top page, then insert a Comment in the relevant location. Making your changes directly in the online proofing interface is the quickest, easiest way to correct and submit your proof.

Please note that changes made to the article in the online proofing interface will be added to the article before publication, but are not reflected in this PDF proof.

If you would prefer to submit your corrections by annotating the PDF proof, please download and submit an annotatable PDF proof by clicking the link below.

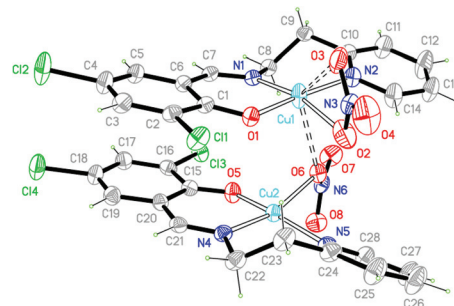
 [Annotate PDF](#)

We have presented the graphical abstract image and text for your article below. This briefly summarises your work, and will be presented with your article online.

1

Copper(II) complexes with tridentate halogen-substituted Schiff base ligands: synthesis, crystal structures and investigating the effect of halogenation, leaving groups and ligand flexibility on antiproliferative activities

Nazanin Kordestani, Hadi Amiri Rudbari,*
Alexandra R. Fernandes,* Luís R. Raposo, André Luz,
Pedro V. Baptista, Giuseppe Bruno, Rosario Scopelliti,
Zohreh Fatemina, Nicola Micale, Nikolay Tumanov,
Johan Wouters, Abolghasem Abbasi Kajani and
Abdol-Khategh Bordbar



To investigate the effect of different halogen substituents and leaving groups and the flexibility of ligands on the anticancer activity of copper complexes, sixteen copper(II) complexes with eight different tridentate Schiff-base ligands containing pyridine and 3,5-halogen substituted phenol moieties were synthesized and characterized by spectroscopic methods.

Q5 Q4

Please check this proof carefully. Our staff will not read it in detail after you have returned it.

Please send your corrections either as a copy of the proof PDF with electronic notes attached or as a list of corrections. **Do not edit the text within the PDF or send a revised manuscript** as we will not be able to apply your corrections. Corrections at this stage should be minor and not involve extensive changes.

Proof corrections must be returned as a single set of corrections, approved by all co-authors. No further corrections can be made after you have submitted your proof corrections as we will publish your article online as soon as possible after they are received.

Please ensure that:

- The spelling and format of all author names and affiliations are checked carefully. You can check how we have identified the authors' first and last names in the researcher information table on the next page. **Names will be indexed and cited as shown on the proof, so these must be correct.**
- Any funding bodies have been acknowledged appropriately and included both in the paper and in the funder information table on the next page.
- All of the editor's queries are answered.
- Any necessary attachments, such as updated images or ESI files, are provided.

Translation errors can occur during conversion to typesetting systems so you need to read the whole proof. In particular please check tables, equations, numerical data, figures and graphics, and references carefully.

Please return your **final** corrections, where possible within **48 hours** of receipt following the instructions in the proof notification email. If you require more time, please notify us by email to dalton@rsc.org.

Funding information

Providing accurate funding information will enable us to help you comply with your funders' reporting mandates. Clear acknowledgement of funder support is an important consideration in funding evaluation and can increase your chances of securing funding in the future.

We work closely with Crossref to make your research discoverable through the Funding Data search tool (<http://search.crossref.org/funding>). Funding Data provides a reliable way to track the impact of the work that funders support. Accurate funder information will also help us (i) identify articles that are mandated to be deposited in **PubMed Central (PMC)** and deposit these on your behalf, and (ii) identify articles funded as part of the **CHORUS** initiative and display the Accepted Manuscript on our web site after an embargo period of 12 months.

Further information can be found on our webpage (<http://rsc.li/funding-info>).

What we do with funding information

We have combined the information you gave us on submission with the information in your acknowledgements. This will help ensure the funding information is as complete as possible and matches funders listed in the Crossref Funder Registry.

If a funding organisation you included in your acknowledgements or on submission of your article is not currently listed in the registry it will not appear in the table on this page. We can only deposit data if funders are already listed in the Crossref Funder Registry, but we will pass all funding information on to Crossref so that additional funders can be included in future.

Please check your funding information

The table below contains the information we will share with Crossref so that your article can be found *via* the Funding Data search tool. **Please check that the funder names and grant numbers in the table are correct and indicate if any changes are necessary to the Acknowledgements text.**

Funder name	Funder's main country of origin	Funder ID (for RSC use only)	Award/grant number
Fundação para a Ciência e a Tecnologia	Portugal	501100001871	Unassigned
Ministério da Ciência, Tecnologia e Ensino Superior	Portugal	501100006111	UIDB/04378/2020

Q1

Researcher information

Please check that the researcher information in the table below is correct, including the spelling and formatting of all author names, and that the authors' first, middle and last names have been correctly identified. **Names will be indexed and cited as shown on the proof, so these must be correct.**

If any authors have ORCID or ResearcherID details that are not listed below, please provide these with your proof corrections. Please ensure that the ORCID and ResearcherID details listed below have been assigned to the correct author. Authors should have their own unique ORCID iD and should not use another researcher's, as errors will delay publication.

Please also update your account on our online [manuscript submission system](#) to add your ORCID details, which will then be automatically included in all future submissions. See [here](#) for step-by-step instructions and more information on author identifiers.

First (given) and middle name(s)	Last (family) name(s)	ResearcherID	ORCID iD
Nazanin	Kordestani		
Hadi	Amiri Rudbari	G-8030-2011	0000-0002-3020-8596
Alexandra R.	Fernandes	C-7465-2011	0000-0003-2054-4438
Luís R.	Raposo	T-3754-2017	0000-0002-8637-346X
André	Luz		
Pedro V.	Baptista		0000-0001-5255-7095

Giuseppe	Bruno		
Rosario	Scopelliti		0000-0001-8161-8715
Zohreh	Fateminia		
Nicola	Micale		
Nikolay	Tumanov	O-5866-2015	0000-0001-6898-9036
Johan	Wouters		
Abolghasem	Abbasi Kajani		
Abdol-Khalegh	Bordbar		0000-0002-0409-1494

Queries for the attention of the authors

Journal: **Dalton Transactions** Paper: **d0dt03962d**

Title: **Copper(II) complexes with tridentate halogen-substituted Schiff base ligands: synthesis, crystal structures and investigating the effect of halogenation, leaving groups and ligand flexibility on antiproliferative activities**

For your information: You can cite this article before you receive notification of the page numbers by using the following format: (authors), Dalton Trans., (year), DOI: 10.1039/d0dt03962d.

Editor's queries are marked like this **Q1**, **Q2**, and for your convenience line numbers are indicated like this 5, 10, 15, ...

Please ensure that all queries are answered when returning your proof corrections so that publication of your article is not delayed.

Query Reference	Query	Remarks
Q1	Funder details have been incorporated in the funder table using information provided in the article text. Please check that the funder information in the table is correct.	
Q2	Please check that the inserted CCDC numbers are correct.	
Q3	Please confirm that the spelling and format of all author names is correct. Names will be indexed and cited as shown on the proof, so these must be correct. No late corrections can be made.	
Q4	The first line of the Abstract has been inserted as the Graphical Abstract text; however, it currently exceeds the space available for the published version. Please check that the text is suitable and trim it so that it is shorter than 250 characters (including spaces).	
Q5	Please check that the inserted Graphical Abstract image is suitable.	
Q6	"Schemes 1 and 2" and their corresponding citations have been relabelled as "Tables 1 and 2" and the subsequent tables have been renumbered. Please check that the renumbering is correct and that all of the citations within the text correspond to the correct table and indicate any changes required.	
Q7	Ref. 1: Please provide the title.	
Q8	Ref. 37: Please provide the last name for the 2nd author.	
Q9	Ref. 54: Please check that the last name for the 1st author is displayed correctly.	

PAPER

Copper(II) complexes with tridentate halogen-substituted Schiff base ligands: synthesis, crystal structures and investigating the effect of halogenation, leaving groups and ligand flexibility on antiproliferative activities†

Cite this: DOI: 10.1039/d0dt03962d

Q3

Nazanin Kordestani,^a Hadi Amiri Rudbari,^{id} *^a Alexandra R. Fernandes,^{id} *^b Luís R. Raposo,^{id} ^b André Luz,^b Pedro V. Baptista,^{id} ^b Giuseppe Bruno,^c Rosario Scopelliti,^{id} ^d Zohreh Fatemina,^a Nicola Micale,^c Nikolay Tumanov,^{id} ^e Johan Wouters,^e Abolghasem Abbasi Kajani^f and Abdol-Khalegh Bordbar^{id} ^g

To investigate the effect of different halogen substituents and leaving groups and the flexibility of ligands on the anticancer activity of copper complexes, sixteen copper(II) complexes with eight different tridentate Schiff-base ligands containing pyridine and 3,5-halogen substituted phenol moieties were synthesized and characterized by spectroscopic methods. Four of these complexes were also characterized by X-ray crystallography. The cytotoxicity of the complexes was determined in three different tumor cell lines (*i.e.* the A2780 ovarian, HCT116 colorectal and MCF7 breast cancer cell line) and in a normal primary fibroblast cell line. Complexes were demonstrated to induce a higher loss of cell viability in the ovarian carcinoma cell line (A2780) with respect to the other two tumor cell lines, and therefore the biological mechanisms underlying this loss of viability were further investigated. Complexes with ligand **L**₁ (containing a 2-pycolylamine-type motif) were more cytotoxic than complexes with **L**₂ (containing a 2-(2-pyridyl)ethylamine-type motif). The loss of cell viability in A2780 tumor cells was observed in the order **Cu(Cl₂-L₁)NO₃** > **Cu(Cl₂-L₁)Cl** > **Cu(Br₂-L₁)Cl** > **Cu(BrCl-L₁)Cl**. All complexes were able to induce reactive oxygen species (ROS) that could be related to the loss of cell viability. Complexes **Cu(BrCl-L₁)Cl** and **Cu(Cl₂-L₁)NO₃** were able to promote A2780 cell apoptosis and autophagy and for complex **Cu(BrCl-L₁)Cl** the increase in apoptosis was due to the intrinsic pathway. **Cu(Cl₂-L₁)Cl** and **Cu(Br₂-L₁)Cl** complexes lead to cellular detachment allowing to correlate with the results of loss of cell viability. Despite the ability of the **Cu(BrCl-L₁)Cl** complex to induce programmed cell death in A2780 cells, its therapeutic window turned out to be low making the **Cu(Cl₂-L₁)NO₃** complex the most promising candidate for additional biological applications.

Received 18th November 2020,

Accepted 14th February 2021

DOI: 10.1039/d0dt03962d

rsc.li/dalton

^aDepartment of Chemistry, University of Isfahan, Isfahan 81746-73441, Iran.

E-mail: hamiri1358@gmail.com, h.a.rudbari@sci.ui.ac.ir

^bUCIBIO, Departamento Ciências da Vida, Faculdade de Ciências e Tecnologia, Universidade NOVA de Lisboa, 2829-516 Caparica, Portugal.

E-mail: ma.fernandes@fct.unl.pt

^cDepartment of Chemical, Biological, Pharmaceutical and Environmental Sciences, University of Messina, Viale Ferdinando Stagno D'Alcontres 31, I-98166 Messina, Italy^dInstitut des Sciences et Ingénierie Chimiques, École Polytechnique Fédérale de Lausanne (EPFL), CH-1015 Lausanne, Switzerland^eDepartment of Chemistry, Namur Institute of Structured Matter, University of Namur, 5000 Namur, Belgium^fApplied Physiology Research Center, Cardiovascular Research Institute, Isfahan University of Medical Sciences, Isfahan, 81746-73461, Iran^gCalifornia Institute for Quantitative Biosciences (QB3), University of California, Berkeley, CA 94720, USA

† Electronic supplementary information (ESI) available. CCDC 1872089–1872092.

For ESI and crystallographic data in CIF or other electronic format see DOI:

10.1039/d0dt03962d

Q2

Introduction

Cancer is the second leading cause of death worldwide and its incidence is increasing.¹ Transition metal complexes with their versatile structures, redox behavior and physicochemical properties have been found to be useful as active agents in chemotherapeutic applications.² The serendipitous discovery of cisplatin as an anticancer drug has initiated the investigation in the medicinal bioinorganic research field. Cisplatin [*cis*-diamminedichlorideplatinum(II)], as one of the foremost and widely used metal-based anticancer drugs,^{3,4} is currently used for the treatment of a variety of cancers.⁵ However, its application is mostly limited by both its side-effects and acquired cellular resistance.^{6,7} Therefore, tremendous efforts have been made for the development of metal-based anticancer compounds with less toxicity and higher efficiency,^{8,9}

particularly biocompatible copper(II) complexes that bind to and cleave DNA under physiological conditions.¹⁰ Copper has a long history of medical use, and its prospective antitumor properties have recently attracted attention because it is thought to be less toxic than nonessential metals such as platinum.^{11,12} Moreover, its complexes with tunable coordination geometry in a redox active environment could find better efficacy at the cellular level.¹³ Since 1969, copper has been found to possess high DNA binding affinity.¹⁴ This binding was dependent on the copper complex size, electron affinity, and geometry of the formed adduct, inducing an irreversible modification of the DNA conformational structure. According to these observations, a large number of copper complexes have been considered as DNA-targeting metallo-drugs.¹⁵ The premise that stoichiometric mixtures of copper ions and organic chelators can form a new class of proteasome inhibitors has been recently investigated by Dou's group.^{16–18} Recent studies have shown that a square-planar Cu(II) complex chelated by an *N,N,O*-tridentate Schiff-base containing phenolic and pyridine rings as coordinating groups has a remarkable capability to cleave DNA.^{19,20} However, 50% of the top leading drugs on the market are halogen-substituted.²¹ In the drug design process, halogen atoms are often introduced in order to increase membrane permeability and to prolong the drug's half-life by delaying the catabolic process, which leads to drug degradation and loss of pharmacological activity in the organism.²² In fact, halogen for hydrogen substitution on aromatic rings of drugs affords compounds where the carbon–halogen bonds are catabolically more stable than the corresponding C–H bonds. Usually, halogen atoms in drugs or drug-like molecules are understood to be involved in non-directional hydrophobic interactions or just pointed into relatively empty spaces or cavities which they tend to occupy without being involved in major stabilizing contacts. However, since potential electron-rich sites such as oxygen, nitrogen, and sulfur atoms as well as aromatic π -electron systems are abundant in proteins, halogen atoms can also form, stabilizing interactions such as halogen bonds with the surrounding amino acids. A recent systemic investigation of halogen bonds in protein–ligand complexes by Hardegger *et al.* showed that halogen bonds can serve as a powerful tool in increasing binding selectivity and binding affinity.²³ Similarly, some metal complexes with the asymmetric *N*-pyridine-*N'*-amine-*O*-phenolate 2,4-di-*X*-6-((pyridine-2-yl-methylamino)methyl)phenol ligands HL_{*x*} (where *X* = H, *tert*-butyl, bromo or iodo) were synthesized by Verani's group.^{24–28} The results showed that the bromo or iodo substituted species were effective against cisplatin-resistant neuroblastoma as well as for a number of other tumors. Furthermore, by comparing the results of some previous reports, it can be concluded that the size of the ring that was formed during the formation of a complex, or, in other words, the ligand flexibility can be effective on anti-cancer properties of the compounds.^{25–29} Finally, to enrich the delivery efficiency and enhance the anticancer activity and selectivity of anticancer metal agents, having good leaving group(s)

on complexes, such as chloride, nitrate and acetate, is necessary, as reported in previous reports.²⁵

The significant aspect of this work is the investigation of the effect of different halogen substituents, the flexibility of ligands and leaving groups on the synthesized copper(II) complexes with *N,N,O*-tridentate Schiff-base containing phenolic and pyridine rings and study of their potential applications in cancer research. For this purpose, 3,5-halogen substituted phenol moieties with similar and different halogens were used to investigate the role of halogen groups in anticancer activity. Two different substituted pyridine amines (2-(2-pyridyl)ethylamine and 2-picolyamine) were employed in order to consider the ligand flexibility, and two kinds of copper(II) salts, *i.e.* (Cu(NO₃)₂·H₂O and CuCl₂·H₂O), were also used to investigate the effect of the leaving group on anticancer activity.

Hence, we have synthesized and characterized eight ligands and sixteen complexes which are depicted in Tables 1 and 2, respectively. These compounds were characterized by elemental analysis and FT-IR and NMR spectroscopy. Molecular structures of four complexes were solved by X-ray crystallography. In order to fulfill the aim of this research work, the antiproliferative potential of the complexes was evaluated on three carcinoma cell lines (MCF-7, A2780 and HCT116) and the cytotoxicity profile on normal human dermal fibroblast cells.

Table 1 All synthesized ligands

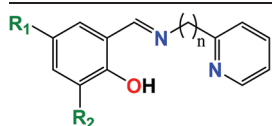
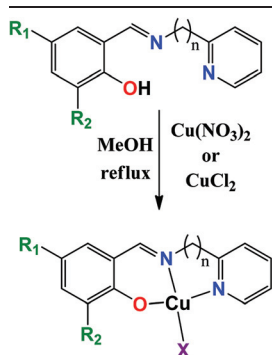
	R ₁	R ₂	<i>n</i>	
	Br	Br	1	Br ₂ -HL ₁
	Cl	Cl	1	Cl ₂ -HL ₁
	I	I	1	I ₂ -HL ₁
	Br	Cl	1	BrCl-HL ₁
	Br	Br	2	Br ₂ -HL ₂
	Cl	Cl	2	Cl ₂ -HL ₂
	I	I	2	I ₂ -HL ₂
	Br	Cl	2	BrCl-HL ₂

Table 2 All synthesized complexes

	R ₁	R ₂	X	<i>N</i>	
	Br	Br	Cl	1	Cu(Br ₂ -L ₁)Cl
	Cl	Cl	Cl	1	Cu(Cl ₂ -L ₁)Cl
	I	I	Cl	1	Cu(I ₂ -L ₁)Cl
	Br	Cl	Cl	1	Cu(BrCl-L ₁)Cl
	Br	Br	NO ₃	1	Cu(Br ₂ -L ₁)NO ₃
	Cl	Cl	NO ₃	1	Cu(Cl ₂ -L ₁)NO ₃
	I	I	NO ₃	1	Cu(I ₂ -L ₁)NO ₃
	Br	Cl	NO ₃	1	Cu(BrCl-L ₁)NO ₃
	Br	Br	Cl	2	Cu(Br ₂ -L ₂)Cl
	Cl	Cl	Cl	2	Cu(Cl ₂ -L ₂)Cl
	I	I	Cl	2	Cu(I ₂ -L ₂)Cl
	Br	Cl	Cl	2	Cu(BrCl-L ₂)Cl
	Br	Br	NO ₃	2	Cu(Br ₂ -L ₂)NO ₃
	Cl	Cl	NO ₃	2	Cu(Cl ₂ -L ₂)NO ₃
	I	I	NO ₃	2	Cu(I ₂ -L ₂)NO ₃
	Br	Cl	NO ₃	2	Cu(BrCl-L ₂)NO ₃

Results and discussion

Synthesis and characterization

The ligands were synthesized by Schiff condensation of 2-hydroxy-3,5 halogen substituted salicylaldehyde with 2-(2-pyridyl)ethylamine and 2-picolylamine in distilled water at room temperature separately, according to our published work (Table 1).³⁰

The synthesis of the Cu(II) complexes was performed using a common procedure, by reaction of a stoichiometric amount of $\text{CuCl}_2 \cdot \text{H}_2\text{O}$ and $\text{Cu}(\text{NO}_3)_2 \cdot \text{H}_2\text{O}$ with the corresponding ligands, in methanol. These reactions yielded distorted square planar mononuclear species in which the metal ion was surrounded by a tridentate ligand (N, N, O) and one leaving group (Cl or NO_3) (Table 2). The sixteen resulting complexes, as green color production, were analyzed by elemental analysis and FT-IR spectroscopy and four of them were studied by X-ray diffraction analysis. The shift of the imine band by complexation suggests coordination *via* the imine nitrogen atom.³⁰ Also the stretching vibration of the phenolic OH group of ligands disappeared in the FT-IR spectra of the complexes.

X-ray crystal structures

Description of the crystal structures $\text{Cu}(\text{Cl}_2\text{-L}_2)\text{NO}_3$, $\text{Cu}(\text{Br}_2\text{-L}_2)\text{NO}_3$ and $\text{Cu}(\text{BrCl-L}_2)\text{NO}_3$. Views of the molecular structures of $\text{Cu}(\text{Cl}_2\text{-L}_2)\text{NO}_3$, $\text{Cu}(\text{Br}_2\text{-L}_2)\text{NO}_3$ and $\text{Cu}(\text{BrCl-L}_2)\text{NO}_3$ complexes with the common atom numbering scheme are shown in Fig. 1–3, respectively. The crystallographic data and selected bond lengths and angles are collected in Tables 3 and 4, respectively. Single crystal X-ray analysis reveals that all complexes crystallize in monoclinic $P2_1/n$ space groups. All three complexes have identical structures. Hence, the bond lengths and angles in the three complexes are comparable to each other.

As shown in Fig. 1–3, two mononuclear complexes connected to each other by an oxygen atom of one nitrate group (O(6)). The Cu(1)–O(6)–Cu(2) angles in $\text{Cu}(\text{Cl}_2\text{-L}_2)\text{NO}_3$, $\text{Cu}(\text{Br}_2\text{-L}_2)\text{NO}_3$ and $\text{Cu}(\text{BrCl-L}_2)\text{NO}_3$ are 96.88(1), 96.11(1) and 96.22(1)°, respectively, and are very near to each other (Table 4). The O(6)–Cu(1) bond distance is 2.5750(1) Å in $\text{Cu}(\text{Cl}_2\text{-L}_2)\text{NO}_3$, 2.5499(1) Å in $\text{Cu}(\text{Br}_2\text{-L}_2)\text{NO}_3$ and 2.5604(5) Å in $\text{Cu}(\text{BrCl-L}_2)\text{NO}_3$ (Table 4). These bond distances in all three structures are in the range of upper values for a long coordination distance in Cu(II) compounds. These distances clearly indicate a relatively weak coordination of O(6) to Cu(1) atom. Without this oxygen–copper interaction, we can assume these binuclear complexes as two mononuclear complexes. Surely, this interaction exists only in solid state and in the solution we cannot see this oxygen–copper weak coordination. Perhaps, one of the reasons for this lack of dimerization is some steric hindrance for the coordination of any of the O-atoms due to the non-planarity of the chelate ring formed by the py- $\text{CH}_2\text{-CH}_2\text{-N=}$ arm of ligands.

Also, the distances between the Cu(1) atom and O-atom (O3) of another nitrate group are 2.5920(1), 2.6823(1) and 2.6673(5) Å in $\text{Cu}(\text{Cl}_2\text{-L}_2)\text{NO}_3$, $\text{Cu}(\text{Br}_2\text{-L}_2)\text{NO}_3$ and $\text{Cu}(\text{BrCl-L}_2)\text{NO}_3$ complexes, respectively (Table 4). These distances also clearly indicate a relatively weak coordination of O(3) to Cu(1) atom. The strong coordination of O(2) and weak coordination of O(3) or, in other words, the asymmetric bidentate coordination of the nitrate (NO_3^-) suggest the localization of the negative charge predominantly on O(2). This is also reflected in the longer N(3)–O(2) bond lengths (1.2848(1) Å in $\text{Cu}(\text{Cl}_2\text{-L}_2)\text{NO}_3$, 1.2908(1) Å in $\text{Cu}(\text{Br}_2\text{-L}_2)\text{NO}_3$ and 1.295(11) Å in $\text{Cu}(\text{BrCl-L}_2)\text{NO}_3$) than the N(3)–O(3) bond lengths (1.2828(1) Å in $\text{Cu}(\text{Cl}_2\text{-L}_2)\text{NO}_3$, 1.2418(1) Å in $\text{Cu}(\text{Br}_2\text{-L}_2)\text{NO}_3$ and 1.231(10) Å in $\text{Cu}(\text{BrCl-L}_2)\text{NO}_3$). Without consideration of these two weak

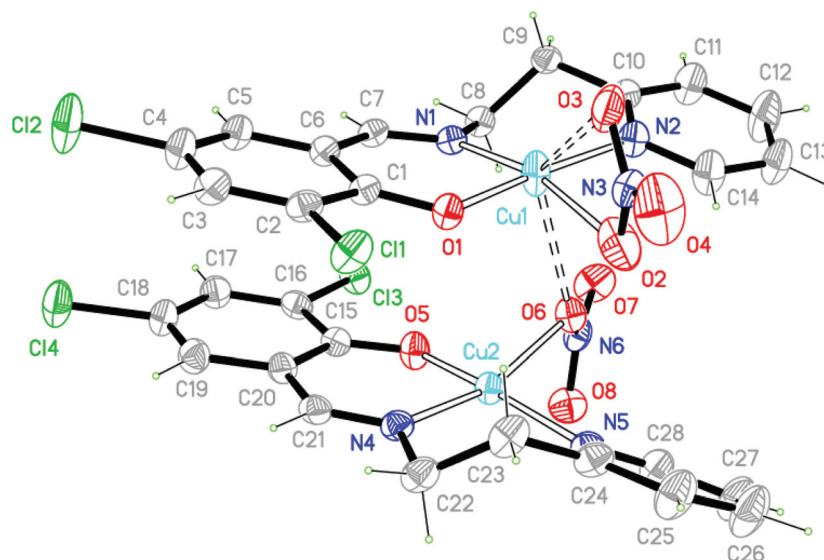


Fig. 1 ORTEP representation of $\text{Cu}(\text{Cl}_2\text{-L}_2)\text{NO}_3$. Displacement ellipsoids are drawn at the 50% probability level and H atoms are shown as small spheres of arbitrary radii. Cu–O short contact is shown as open dashed lines. One NO_3^- groups are disordered over two sites and refined with site occupancy factors 0.73 : 0.27. Only the major component of the disordered NO_3^- group is shown.

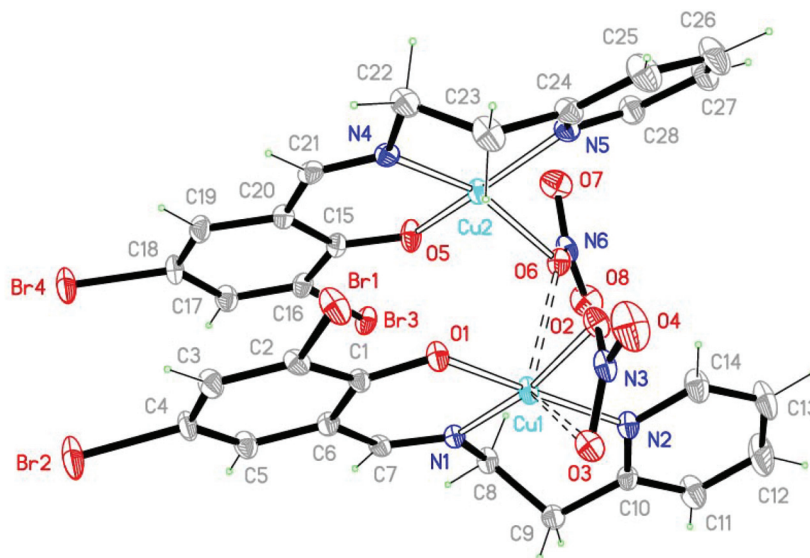


Fig. 2 ORTEP representation of $\text{Cu}(\text{Br}_2\text{-L}_2)\text{NO}_3$. Displacement ellipsoids are drawn at the 50% probability level and H atoms are shown as small spheres of arbitrary radii. Cu–O short contact is shown as open dashed lines.

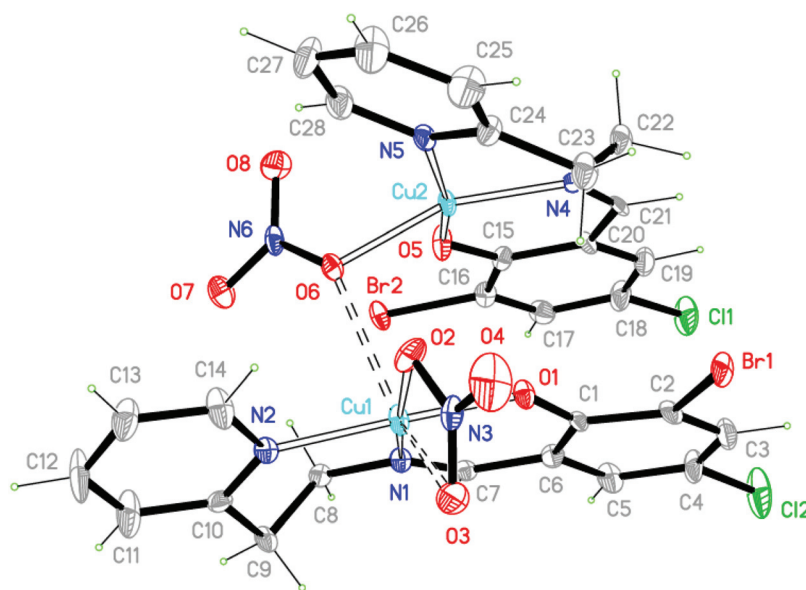


Fig. 3 ORTEP representation of $\text{Cu}(\text{BrCl-L}_2)\text{NO}_3$. Displacement ellipsoids are drawn at the 50% probability level and H atoms are shown as small spheres of arbitrary radii. Cu–O short contact is shown as open dashed lines.

oxygen–copper interactions, $\text{Cu}(1)\text{-O}(3)$ and $\text{Cu}(1)\text{-O}(6)$, the two copper centers ($\text{Cu}(1)$ and $\text{Cu}(2)$) exhibit distorted square planar geometry and consist of one tridentate Schiff-base ligand for each copper center. The coordinating sites of copper atoms are occupied by one phenolate oxygen, one imine nitrogen and one pyridine-N atom of the mono-negative tridentate Schiff-base ligand. The remaining site is occupied by one oxygen atom of the nitrate group.

The sum (Σ) of the six inter-bond angles in four coordinated complexes is a criterion for the deviation amount in square planar geometry. The sum (Σ) of the six inter-bond

angles for the $\text{Cu}(1)$ center is 699.7 , 703.4 and 703.4° for $\text{Cu}(\text{Cl}_2\text{-L}_2)\text{NO}_3$, $\text{Cu}(\text{Br}_2\text{-L}_2)\text{NO}_3$ and $\text{Cu}(\text{BrCl-L}_2)\text{NO}_3$ complexes, respectively, while the sum (Σ) of the six inter-bond angles for the $\text{Cu}(2)$ center is 689.6 , 689.5 and 689.1° for $\text{Cu}(\text{Cl}_2\text{-L}_2)\text{NO}_3$, $\text{Cu}(\text{Br}_2\text{-L}_2)\text{NO}_3$ and $\text{Cu}(\text{BrCl-L}_2)\text{NO}_3$ complexes, respectively (Table 4). It deviates from the ideal angle of 720° in ideal square planar geometry, suggesting that the copper(II) centers have distorted square planar geometry, and that the deviation of square planar geometry in the $\text{Cu}(2)$ center is greater than that in the $\text{Cu}(1)$ center. The reason for this greater deviation of square planar geometry around $\text{Cu}(2)$ is the existence of

Table 3 Crystal data and structure refinements

	Cu(Cl₂-L₂)NO₃ C ₂₈ H ₂₂ Cl ₄ Cu ₂ N ₆ O ₈	Cu(BrCl-L₂)NO₃ C ₂₈ H ₂₂ Br ₂ Cl ₂ Cu ₂ N ₆ O ₈	Cu(Br₂-L₂)NO₃ C ₂₈ H ₂₂ Br ₄ Cu ₂ N ₆ O ₈	Cu(I₂-L₂)Cl C ₁₄ H ₁₁ ClCuI ₂ N ₂ O
Empirical formula				
Formula weight	839.39	928.31	1017.23	576.04
Temperature (K)	140.00(10)	120(2)	140.00(10)	100.01(10)
Wavelength (Å)	1.54184	0.71073	1.54184	0.71073
Crystal system	Monoclinic	Monoclinic	Monoclinic	Triclinic
Space group	<i>P</i> 2 ₁ / <i>n</i>	<i>P</i> 2 ₁ / <i>n</i>	<i>P</i> 2 ₁ / <i>n</i>	<i>P</i> 1
Unit cell dimensions				
<i>a</i> (Å)	14.1249(3)	14.3113(6)	14.25361(14)	7.6342(4)
<i>b</i> (Å)	10.0756(3)	10.1603(12)	10.15411(9)	8.3051(6)
<i>c</i> (Å)	21.5993(6)	21.679(4)	21.8598(2)	13.3598(10)
α (°)	90	90	90	74.533(6)
β (°)	90.8729(18)	91.547(7)	90.3364(9)	88.995(5)
γ (°)	90	90	90	79.331(5)
Volume (Å ³)	3073.59(14)	3151.1(7)	3163.77(5)	801.80(9)
<i>Z</i>	4	4	4	2
Density (calculated) (Mg m ⁻³)	1.814	1.957	2.136	2.386
Absorption coefficient (mm ⁻¹)	5.453	4.117	8.110	5.377
<i>F</i> (000)	1688	1832	1976	538
Theta range for data collection (°)	3.713 to 75.978	1.423 to 30.000	3.692 to 75.303	3.379 to 29.597
Index ranges	-17 ≤ <i>h</i> ≤ 17 -12 ≤ <i>k</i> ≤ 12 -26 ≤ <i>l</i> ≤ 26	-20 ≤ <i>h</i> ≤ 19 -14 ≤ <i>k</i> ≤ 14 -30 ≤ <i>l</i> ≤ 30	-11 ≤ <i>h</i> ≤ 17 -12 ≤ <i>k</i> ≤ 12 -27 ≤ <i>l</i> ≤ 27	-10 ≤ <i>h</i> ≤ 10 -10 ≤ <i>k</i> ≤ 10 -8 ≤ <i>l</i> ≤ 18
Reflections collected	8568	42 539	22 226	3771
Independent reflections	8568	9213	6440	3771
Data completeness (%)	98.5	99.5	100.0	99.1
Absorption correction	Gaussian	Semi-empirical from equivalents	Analytical	Gaussian
Refinement method	Full-matrix least-squares on <i>F</i> ²	Full-matrix least-squares on <i>F</i> ²	Full-matrix least-squares on <i>F</i> ²	Full-matrix least-squares on <i>F</i> ²
Data/restraints/parameters	8568/87/436	9213/0/428	6440/0/435	3771/0/191
Goodness-of-fit on <i>F</i> ²	1.050	1.034	1.101	1.142
Final <i>R</i> indices [<i>I</i> > 2σ(<i>I</i>)]	<i>R</i> ₁ = 0.0452 <i>wR</i> ₂ = 0.1350	<i>R</i> ₁ = 0.0786 <i>wR</i> ₂ = 0.2150	<i>R</i> ₁ = 0.0272 <i>wR</i> ₂ = 0.0724	<i>R</i> ₁ = 0.0418 <i>wR</i> ₂ = 0.0751
<i>R</i> indices (all data)	<i>R</i> ₁ = 0.0483 <i>wR</i> ₂ = 0.1378	<i>R</i> ₁ = 0.0953 <i>wR</i> ₂ = 0.2335	<i>R</i> ₁ = 0.0281 <i>wR</i> ₂ = 0.0730	<i>R</i> ₁ = 0.0568 <i>wR</i> ₂ = 0.0816
Largest diff. peak and hole (e Å ⁻³)	0.483 and 0.1378	3.305 and -0.930	0.852 and -0.517	1.595 and -0.949
CCDC number	1872092	1872091	1872090	1872089

O(6) of the N(4)N(5)O(5) plane with a deviation value of 0.915, 0.910 and 0.925 Å for **Cu(Cl₂-L₂)NO₃**, **Cu(Br₂-L₂)NO₃** and **Cu(BrCl-L₂)NO₃** complexes, respectively.

In all complexes, the six-membered chelate ring formed by the salicylaldimine fragment of the ligand is planar (rms deviation: 0.078 and 0.038 Å for **Cu(Cl₂-L₂)NO₃**, 0.058 and 0.029 Å for **Cu(Br₂-L₂)NO₃**, 0.059 and 0.038 Å for **Cu(BrCl-L₂)NO₃**. However the metal ion is displaced by 0.305 and 0.152 Å in **Cu(Cl₂-L₂)NO₃**, 0.220 and 0.116 Å in **Cu(Br₂-L₂)NO₃**, and 0.220 and 0.153 Å in **Cu(BrCl-L₂)NO₃** from the plane constituted by the remaining five atoms. Thus in these complexes, the chelate ring is folded along the O(1), N(1) line in the O(1)-C(1)-C(6)-C(7)-N(1)-Cu(1) ring and along the O(5), N(4) line in the O(5)-C(15)-C(20)-C(21)-N(4)-Cu(2) ring and they have a half-chair like conformation. As expected, the second six-membered chelate ring formed by the py-CH₂-CH₂-N= arm of the ligand is not planar due to the two methylene groups in all complexes. Interestingly, this chelate ring has a half-chair conformation in all complexes (Fig. 4). In the half-chair conformation, one of the methylene C-atoms (C(9) in Cu(1)-N(1)-

C(8)-C(9)-C(10)-N(2) and C(23) in Cu(2)-N(4)-C(22)-C(23)-C(24)-N(5)) is displaced by 0.685 and 0.754 Å in **Cu(Cl₂-L₂)NO₃**, 0.687 and 0.768 Å in **Cu(Br₂-L₂)NO₃**, and 0.665 and 0.767 Å in **Cu(BrCl-L₂)NO₃** from the mean plane constituted by Cu(1)-N(1)-C(8)-C(9)-C(10)-N(2) and Cu(2)-N(4)-C(22)-C(23)-C(24)-N(5) rings. The C=N bond distances are in the range of 1.277(3)-1.297(10) Å for reported structures, which is consistent with the C=N bond when coordinated to a metal center (Table 4).³¹ With considering two weak oxygen-copper interactions, Cu(1)-O(3) and Cu(1)-O(6), the Cu(1) atom is in a distorted octahedral environment, where three donor atoms of the mono-negative tridentate Schiff-base ligand (N(1), N(2) and O(1)) and one oxygen atom of the nitrate group (O(2)) form a square planar arrangement around the Cu(1) atom and the two oxygen atoms of two different nitrate groups weakly coordinate to the Cu(1) at the axial positions. As shown in Fig. 2, the O(3) atom has excessive deviation from axial positions. Surely, this excessive deviation is due to the required angles for the nitrate group (O-N-O angle in NO₃⁻ = 60°).

Table 4 Selected bond lengths (Å) and angles (°) for $\text{Cu}(\text{Cl}_2\text{-L}_2)\text{NO}_3$, $\text{Cu}(\text{Br}_2\text{-L}_2)\text{NO}_3$, $\text{Cu}(\text{BrCl-L}_2)\text{NO}_3$ and $\text{Cu}(\text{I}_2\text{-L}_2)\text{Cl}$

	$\text{Cu}(\text{Cl}_2\text{-L}_2)\text{NO}_3$	$\text{Cu}(\text{BrCl-L}_2)\text{NO}_3$	$\text{Cu}(\text{Br}_2\text{-L}_2)\text{NO}_3$	$\text{Cu}(\text{I}_2\text{-L}_2)\text{Cl}$
Bond lengths (Å)				
Cu(1)–O(1)	1.915(2)	1.931(6)	1.9223(16)	1.903(4)
Cu(1)–O(2)	2.071(9)	2.042(6)	2.2.0267(17)	—
Cu(1)–O(3)	2.5920(1)	2.6673(5)	2.6823(1)	—
Cu(1)–O(6)	2.5750(1)	2.5604(5)	2.5499(1)	—
Cu(1)–N(1)	1.952(3)	1.963(6)	1.9583(18)	1.973(5)
Cu(1)–N(2)	2.023(3)	2.048(7)	2.0407(19)	1.987(5)
Cu(2)–O(5)	1.882(3)	1.993(7)	1.8813(17)	—
Cu(2)–O(6)	1.998(2)	2.010(5)	1.9997(16)	—
Cu(2)–N(4)	1.939(3)	1.945(7)	1.9445(19)	—
Cu(2)–N(5)	1.984(3)	1.993(7)	1.989(2)	—
N(1)–C(7)	1.281(5)	1.285(10)	1.277(3)	1.286(8)
N(4)–C(21)	1.284(5)	1.297(10)	1.285(3)	—
Cu(1)–Cl(1)	—	—	—	2.2460(17)
Bond angles (°)				
O(1)–Cu(1)–N(1)	91.72(11)	91.5(2)	91.68(7)	91.14(19)
O(1)–Cu(1)–O(2)	80.54(15)	81.5(2)	81.33(7)	—
N(1)–Cu(1)–O(2)	166.61(15)	170.3(3)	170.52(7)	—
O(1)–Cu(1)–N(2)	172.77(12)	172.7(3)	172.47(7)	158.7(2)
N(1)–Cu(1)–N(2)	95.46(12)	94.8(3)	94.96(8)	95.3(2)
O(2)–Cu(1)–N(2)	92.57(16)	92.6(3)	92.45(7)	—
O(5)–Cu(2)–N(4)	93.77(12)	93.9(3)	93.83(8)	—
O(5)–Cu(2)–N(5)	165.11(12)	165.1(3)	165.79(8)	—
N(4)–Cu(2)–N(5)	95.92(12)	96.2(3)	95.98(8)	—
O(5)–Cu(2)–O(6)	84.65(11)	84.3(2)	84.49(7)	—
N(4)–Cu(2)–O(6)	160.16(11)	159.6(3)	159.61(7)	—
N(5)–Cu(2)–O(6)	89.98(11)	90.0(3)	89.81(7)	—
Cu(1)–O(6)–Cu(2)	96.88(1)	96.22(1)	96.11(1)	—

One of the interesting interactions in crystal packing of all the complexes is the existence of intermolecular halogen bonds (X-bonds). Halogen bonds (X-bonds) are interactions that occur between an organic halide (–Cl, –Br, –I) and a bound electronegative atom (Lewis base), such as oxygen, nitrogen, or sulfur; the former of these is referred to as the X-bond donor while the latter is called the X-bond acceptor.^{32,33} Most of the halogen bonds in reported complexes involved halogens bound to aromatic groups. Halogen bonds involving aromatic rings are generally stronger than those involving aliphatic chains because aromatic moieties have electron-withdrawing properties that lead to larger σ -holes.

As we can see for example for $\text{Cu}(\text{BrCl-L}_2)\text{NO}_3$ in Fig. 5, only halogens in the *para* position can involve in intramolecular halogen bonds with one oxygen of the nitrate group in the nearest neighbor molecule (O3). These X...O contacts are smaller than the sum of Bondi's van der Waals radii of halogens (3.180 Å (Cl(4)...O(3)) for $\text{Cu}(\text{Cl}_2\text{-L}_2)\text{NO}_3$, 3.209 Å (Br(4)...O(3)) for $\text{Cu}(\text{Br}_2\text{-L}_2)\text{NO}_3$ and 3.185 Å (Cl(1)...O(3)) for $\text{Cu}(\text{BrCl-L}_2)\text{NO}_3$. The vdW radii for Br, Cl, and O atoms are 1.85, 1.75, and 1.52 Å, respectively, and the corresponding sum of the vdW radii is Br + O = 3.37 and Cl + O = 3.27 Å.

Description of the crystal structure $\text{Cu}(\text{I}_2\text{-L}_2)\text{Cl}$. Complex $\text{Cu}(\text{I}_2\text{-L}_2)\text{Cl}$ crystallizes in the triclinic $P\bar{1}$ space group such that the asymmetric unit contains one complex molecule. A representative molecular structure along with a selected atom numbering scheme is depicted in Fig. 6, while the crystal structure refinement data and important bond distances and angles are given in Tables 3 and 4, respectively.

The Cu(II) ion is four-coordinate forming a distorted square planar coordination sphere, in which three positions are occupied by two N atoms and one O atom from the mono-negative tridentate Schiff-base ligand, forming five- and six-membered chelate rings, and the other one coming from a coordinated chloride ion. The CuN_2O unit is located in a well plane with a mean deviation of 0.133 Å, while the chloride ion is obvious out of the above plane with a deviation value of 1.413 Å. Similar to $\text{Cu}(\text{Cl}_2\text{-L}_2)\text{NO}_3$, $\text{Cu}(\text{Br}_2\text{-L}_2)\text{NO}_3$ and $\text{Cu}(\text{BrCl-L}_2)\text{NO}_3$ complexes, the five- and six-membered chelate rings in $\text{Cu}(\text{I}_2\text{-L}_2)\text{Cl}$ have half-chair conformation. The bond distances of Cu–O, Cu–N and Cu–Cl are in the normal range compared to the reported complexes containing the analogous unsymmetrical tridentate Schiff-base ligands.^{19,31}

The sum (Σ) of the six inter-bond angles for $\text{Cu}(\text{I}_2\text{-L}_2)\text{Cl}$ is 682.4°, which deviates from the ideal angle of 720° in ideal square planar geometry, suggesting that the geometry around copper(II) is distorted square planar. Also, the *cis* angles in the basal plane involving the phenolate oxygen and imine nitrogen (O(1)–Cu(1)–N(1), 91.14(19)°) and that involving imine nitrogen and pyridine nitrogen (N(1)–Cu(1)–N(2), 95.3(2)°) deviate from the ideal value of 90°, suggesting that the square planar coordination geometry in $\text{Cu}(\text{I}_2\text{-L}_2)\text{Cl}$ is slightly distorted due to the chelate effect. The C=N bond distance is 1.286(8) Å (N1=C7), which is consistent with a slight elongation of the C=N double bond when coordinated to a late metal center.³⁴

As we can see in Fig. 7, there is intermolecular halogen-halogen type I interaction in the $\text{Cu}(\text{I}_2\text{-L}_2)\text{Cl}$ complex.³⁵ The

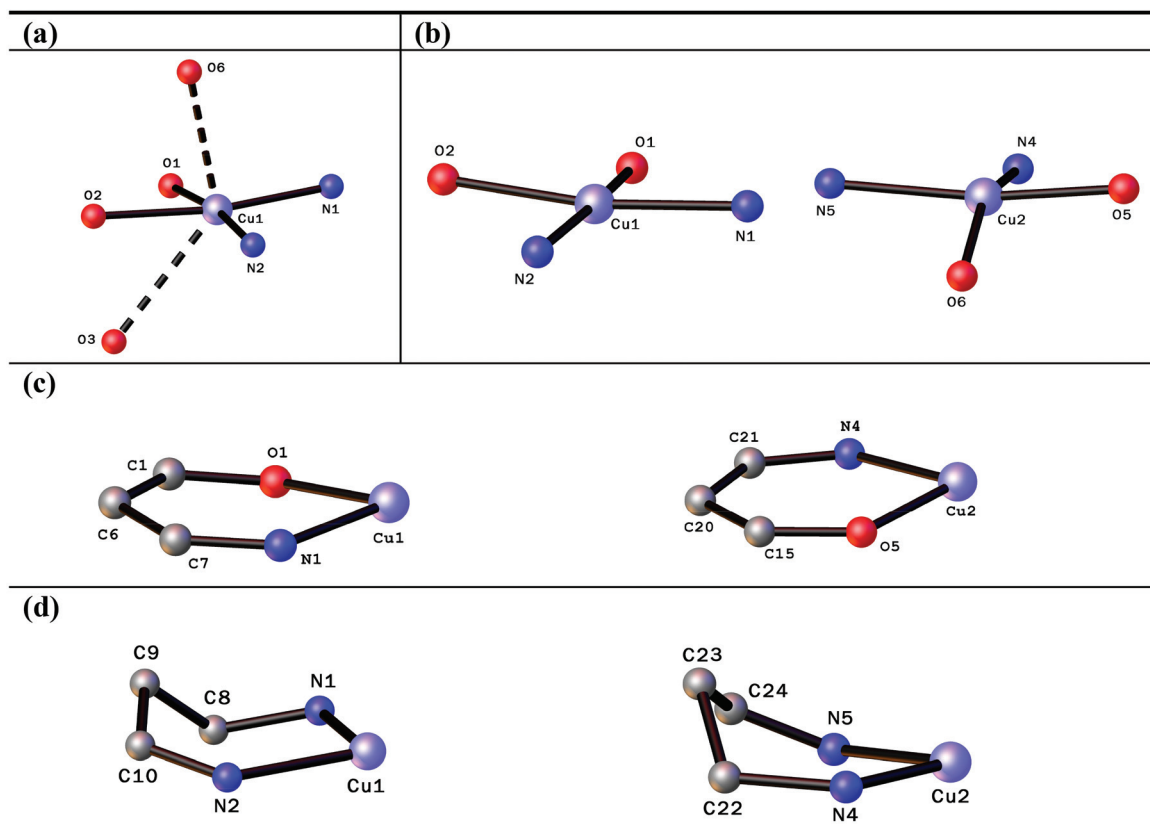


Fig. 4 (a) Coordination environments around atoms Cu(1) with considering weak oxygen–copper interaction; (b) coordination environments around atoms Cu(1) and Cu(2) without considering weak oxygen–copper interaction; (c) half-chair like conformation of the chelate rings formed by the salicyaldimine fragment of ligands; (d) the half-chair conformation of the chelate rings formed by the py–CH₂–CH₂–N= arm of ligands.

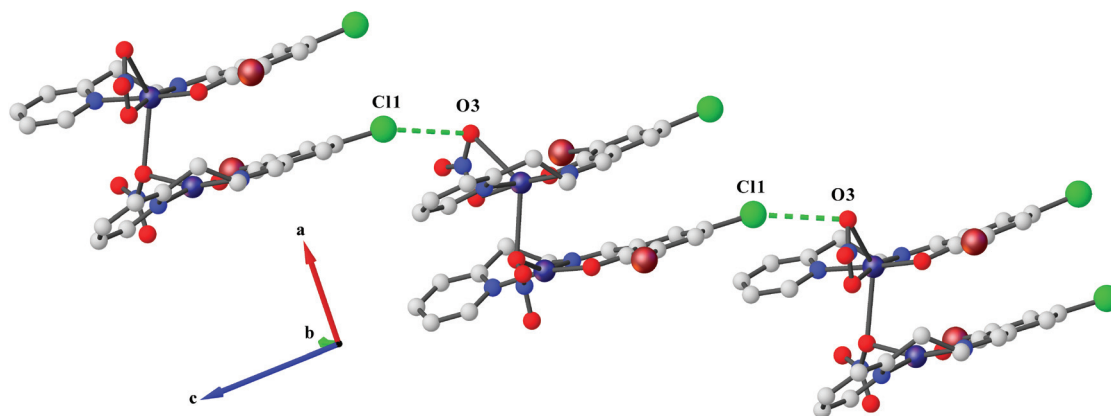


Fig. 5 Halogen bonds (X-bonds) in Cu(BrCl-L₂)NO₃.

halogen atoms in the *ortho* and *para* positions are involved in the halogen–halogen interaction with *ortho* and *para* halogens of another molecule, respectively, with an I⋯I distance of 3.754 Å for I_{ortho}⋯I_{ortho} interaction and 3.862 Å for I_{para}⋯I_{para} interaction. This should be noted that the vdW radius for I atoms is 1.98 Å and the corresponding sum of the vdW radii is I + I = 3.96 Å. Then, these I⋯I contacts are smaller than the

sum of Bondi's van der Waals radii of halogens. A statistical study proved that at distances inferior to the sum of van der Waals radii type I interactions are dominant, while at distances close to the value of that sum halogen bonds prevail. However, when the contact distance is superior to the van der Waals radii sum, type I becomes more frequent, particularly for I⋯I contacts.³⁶

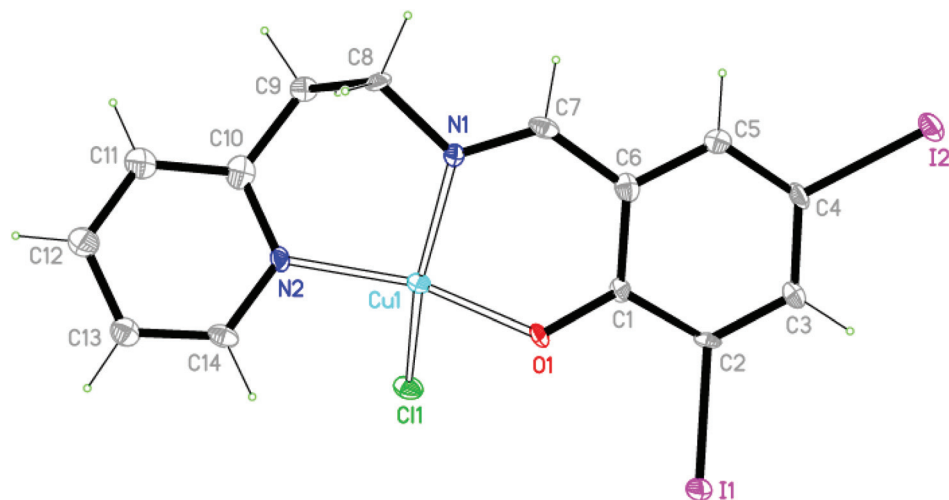


Fig. 6 ORTEP representation of $\text{Cu}(\text{I}_2\text{-L}_2)\text{Cl}$. Displacement ellipsoids are drawn at the 50% probability level and H atoms are shown as small spheres of arbitrary radii.

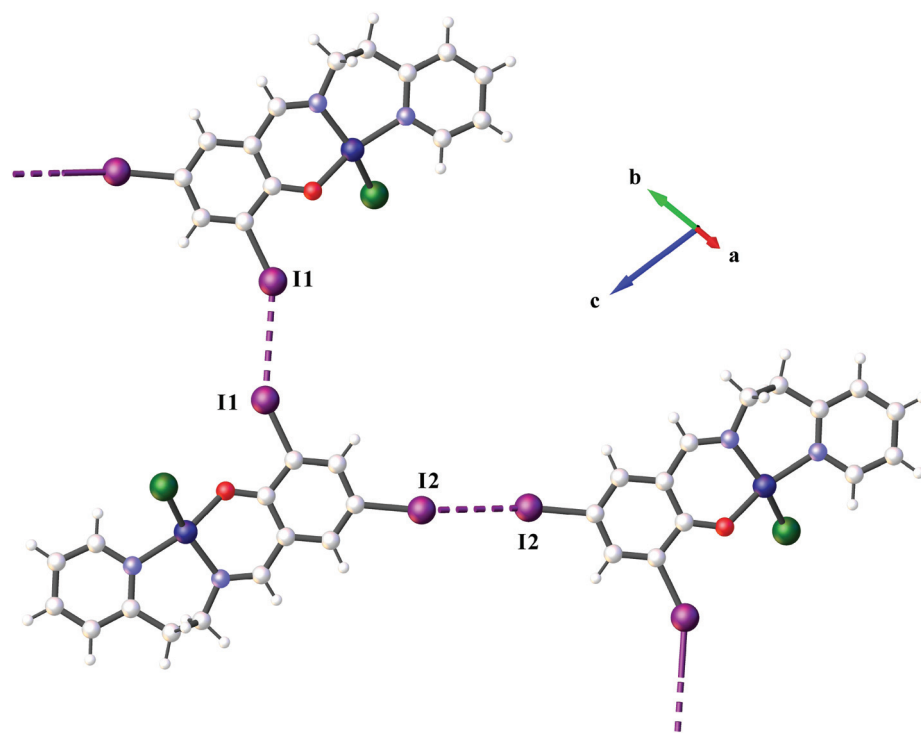


Fig. 7 A side view representation of $\text{Cu}(\text{I}_2\text{-L}_2)\text{Cl}$, showing the association of the adjacent molecules through halogen...halogen interactions ($\text{I}(1)\cdots\text{I}(1)$ or $\text{I}_{ortho}\cdots\text{I}_{ortho}$ distance: 3.754 Å; $\text{I}(2)\cdots\text{I}(2)$ or $\text{I}_{para}\cdots\text{I}_{para}$ distance: 3.862 Å).

Biological assays. Antiproliferative potential and biological mechanisms triggered by the complexes

The antiproliferative effects of $\text{Cu}(\text{II})$ complexes were evaluated in three human cancer cell lines, namely ovarian carcinoma (A2780), colorectal carcinoma (HCT116) and breast adenocarcinoma (MCF7) using the MTS assay. Amongst all sixteen complexes, $\text{Cu}(\text{Cl}_2\text{-L}_1)\text{Cl}$, $\text{Cu}(\text{Br}_2\text{-L}_1)\text{Cl}$, $\text{Cu}(\text{BrCl-L}_1)\text{Cl}$ and Cu

$(\text{Cl}_2\text{-L}_1)\text{NO}_3$ complexes induce a higher antiproliferative activity in A2780 cells compared to HCT116 cells (Fig. 8 and ESI Fig. S1 and Table S1†). In contrast, in MCF7 cells only the $\text{Cu}(\text{Cl}_2\text{-L}_1)\text{NO}_3$ complex, the one with the strongest antiproliferative activity in all tumor cell lines, shows a significant antiproliferative activity (ESI Fig. S1†). It is interesting to note that complexes with L_1 appear to be more active than complexes with L_2 (Fig. 8, Table 5 and ESI Fig. S1 and Table S1†). The six-

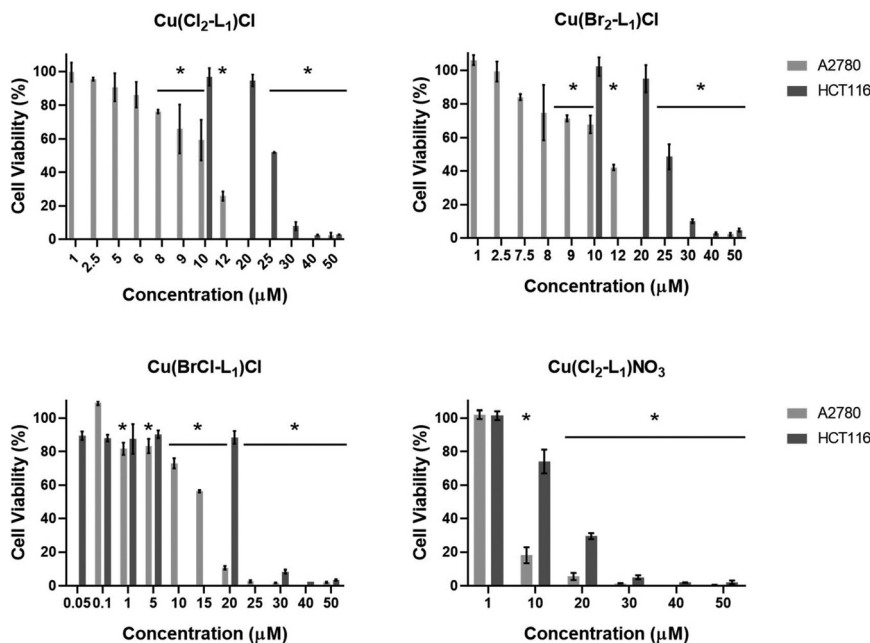


Fig. 8 Antiproliferative effect of complexes $\text{Cu}(\text{Cl}_2\text{-L}_1)\text{Cl}$, $\text{Cu}(\text{Br}_2\text{-L}_1)\text{Cl}$, $\text{Cu}(\text{BrCl-L}_1)\text{Cl}$ and $\text{Cu}(\text{Cl}_2\text{-L}_1)\text{NO}_3$ in A2780 (light grey) and HCT116 (dark grey) cancer cell lines exposed to increasing concentrations of each complex for 48 h evaluated by the MTS method. The vehicle control condition was DMSO 0.1% (v/v) (negative control). The results shown are expressed as the mean \pm SD from three independent assays. The symbol * indicates that p -value < 0.05.

Table 5 Values of relative IC_{50} (μM) in HCT116, A2780 and MCF7 cancer lines and in human normal primary dermal fibroblasts. n.d. – not determined

Cell lines	$\text{Cu}(\text{Cl}_2\text{-L}_1)\text{Cl}$ (μM)	$\text{Cu}(\text{Br}_2\text{-L}_1)\text{Cl}$ (μM)	$\text{Cu}(\text{BrCl-L}_1)\text{Cl}$ (μM)	$\text{Cu}(\text{Cl}_2\text{-L}_1)\text{NO}_3$ (μM)	Cisplatin (μM)
HCT116	25.5 ± 5.52	25.2 ± 7.67	29.1 ± 7.35	18.1 ± 1.78	15.6 ± 0.6 (ref. 41)
A2780	10.1 ± 2.77	11.0 ± 1.85	13.5 ± 3.31	4.2 ± 2.2	3.4 ± 0.2 (ref. 42)
MCF7	43.4 ± 8.73	>50	44.2 ± 4.06	29.9 ± 6.86	>50
Fibroblasts	31.6 ± 5.19	14.8 ± 8.44	25.17 ± 9.50	34.0 ± 6.26	8.8 ± 0.9

membered chelate ring formed by the $\text{py-CH}_2\text{-CH}_2\text{-N=}$ arm of ligand L_2 , unlike five-membered chelate ring in ligand L_1 ,^{37–39} is not planar due to the two methylene groups in all complexes and might make it difficult for complexes to exhibit cytotoxic activity within cells (Fig. 1–3 and 6). The loss of cell viability in A2780 tumor cells was observed in the order $\text{Cu}(\text{Cl}_2\text{-L}_1)\text{NO}_3 > \text{Cu}(\text{Cl}_2\text{-L}_1)\text{Cl} > \text{Cu}(\text{Br}_2\text{-L}_1)\text{Cl} > \text{Cu}(\text{BrCl-L}_1)\text{Cl}$ (Fig. 8 and Table 5). Interestingly, independently of the ligand (L_1 or L_2), the order of cytotoxicity is $\text{Cu}(\text{Cl}_2\text{-L}_n)\text{X} > \text{Cu}(\text{Br}_2\text{-L}_n)\text{X} > \text{Cu}(\text{BrCl-L}_n)\text{X} \sim \text{Cu}(\text{I}_2\text{-L}_n)\text{X}$ (where L_n : L_1 or L_2 and X: Cl or NO_3) and it seems that the cytotoxic activity might be correlated with the electronegativity of the R_1/R_2 substitutions ($\text{Cl}_2 > \text{Br}_2 > \text{I}_2$). Compared with cisplatin, $\text{Cu}(\text{Cl}_2\text{-L}_1)\text{NO}_3$ displayed a similar IC_{50} value, and $\text{Cu}(\text{Cl}_2\text{-L}_1)\text{Cl}$ and $\text{Cu}(\text{Br}_2\text{-L}_1)\text{Cl}$ showed IC_{50} values 3-fold higher (Table 5). When we compare the effect of the leaving group (X = NO_3 or Cl) in complexes $\text{Cu}(\text{Cl}_2\text{-L}_1)\text{X}$ biological activity, a decreased cytotoxic activity is observed for X = Cl that might be correlated with NO_3 being an easier leaving group compared to Cl ⁴⁰ and/or due to a different internalization within cells (see the below discussion).

To evaluate the effect of these complexes in normal human cells, human primary dermal fibroblasts were also exposed to increasing concentrations of the complexes (Fig. 9). As observed in Fig. 9 and Table 5, complex $\text{Cu}(\text{Br}_2\text{-L}_1)\text{Cl}$ induces a higher antiproliferative activity compared to the other three complexes $\text{Cu}(\text{BrCl-L}_1)\text{Cl}$, $\text{Cu}(\text{Cl}_2\text{-L}_1)\text{Cl}$ and $\text{Cu}(\text{BrCl-L}_1)\text{NO}_3$ (with $\text{Cu}(\text{BrCl-L}_1)\text{Cl} > \text{Cu}(\text{Cl}_2\text{-L}_1)\text{Cl} > \text{Cu}(\text{Cl}_2\text{-L}_1)\text{NO}_3$). Considering that the IC_{50} of the complex $\text{Cu}(\text{Br}_2\text{-L}_1)\text{Cl}$ in dermal fibroblasts is very similar to the IC_{50} in A2780 (Table 5), no therapeutic window exists for its application without inducing normal cells cytotoxicity.

If we calculate the *in vitro* selectivity of complexes in A2780 tumor cells compared to normal cells it is clear that complex $\text{Cu}(\text{Cl}_2\text{-L}_1)\text{NO}_3$ is the most promising with a higher therapeutic window followed by $\text{Cu}(\text{Cl}_2\text{-L}_1)\text{Cl}$ (higher SI; Table 6).

It is interesting to note that this higher SI for $\text{Cu}(\text{Cl}_2\text{-L}_1)\text{NO}_3$ followed by $\text{Cu}(\text{Cl}_2\text{-L}_1)\text{Cl}$ seems to be highly dependent on the higher cytotoxic activity of both complexes ($\text{Cu}(\text{Cl}_2\text{-L}_1)\text{NO}_3 > \text{Cu}(\text{Cl}_2\text{-L}_1)\text{Cl}$) in A2780 cells (since their IC_{50} values in normal fibroblasts are similar). In contrast, the lower SI for $\text{Cu}(\text{Br}_2\text{-L}_1)$

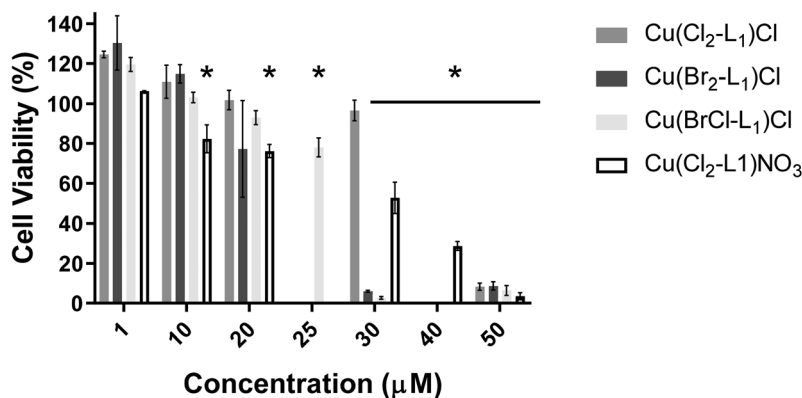


Fig. 9 Cytotoxicity of complexes $\text{Cu}(\text{Cl}_2\text{-L}_1)\text{Cl}$, $\text{Cu}(\text{Br}_2\text{-L}_1)\text{Cl}$, $\text{Cu}(\text{BrCl-L}_1)\text{Cl}$ and $\text{Cu}(\text{Cl}_2\text{-L}_1)\text{NO}_3$ in normal human dermal fibroblasts exposed to increasing concentrations of each complex for 48 h evaluated by the MTS method. The vehicle control condition was DMSO 0.1% (v/v) (negative control). The results shown are expressed as the mean \pm SD from three independent assays. The symbol * indicates that p -value < 0.05 .

Table 6 Selectivity index (SI) of $\text{Cu}(\text{II})$ complexes and cisplatin in A2780 cells compared to normal primary dermal fibroblasts

	$\text{Cu}(\text{Cl}_2\text{-L}_1)\text{Cl}$	$\text{Cu}(\text{Br}_2\text{-L}_1)\text{Cl}$	$\text{Cu}(\text{BrCl-L}_1)\text{Cl}$	$\text{Cu}(\text{Cl}_2\text{-L}_1)\text{NO}_3$	Cisplatin
SI	3.1	1.3	1.5	8.1	2.6

Cl and $\text{Cu}(\text{BrCl-L}_1)\text{Cl}$ is due to their higher levels of cytotoxicity in normal fibroblasts. Moreover, $\text{Cu}(\text{Cl}_2\text{-L}_1)\text{NO}_3$ and $\text{Cu}(\text{Cl}_2\text{-L}_1)\text{Cl}$ show a higher SI compared to cisplatin that might be attributed to the higher cytotoxicity (lower IC_{50}) of cisplatin in normal fibroblasts (Tables 5 and 6 and ESI Fig. S2†). Considering the higher sensitivity of the complexes in the ovarian cancer cell line, A2780, this cell line was selected for further studies (Fig. 8 and Table 5).

To further characterize the cell death mechanisms responsible for the decrease of A2780 cell viability in the presence of the complexes, $\text{Cu}(\text{Cl}_2\text{-L}_1)\text{Cl}$, $\text{Cu}(\text{Br}_2\text{-L}_1)\text{Cl}$, $\text{Cu}(\text{BrCl-L}_1)\text{Cl}$ and

$\text{Cu}(\text{Cl}_2\text{-L}_1)\text{NO}_3$, cells were exposed to the IC_{50} concentrations (Table 5) of each complex for 48 h and analyzed for the presence of cells in apoptosis (early or late) and necrosis (Fig. 10).

Our results indicate that the exposure of A2780 cells to the IC_{50} concentrations of $\text{Cu}(\text{Br}_2\text{-L}_1)\text{Cl}$, $\text{Cu}(\text{BrCl-L}_1)\text{Cl}$ and $\text{Cu}(\text{Cl}_2\text{-L}_1)\text{NO}_3$ led to a statistically significant increase of cells in late apoptosis when compared to the DMSO control (0.6% in cells exposed to $\text{Cu}(\text{Cl}_2\text{-L}_1)\text{Cl}$, 0.7% in cells exposed to $\text{Cu}(\text{Br}_2\text{-L}_1)\text{Cl}$, 38.2% in cells exposed to $\text{Cu}(\text{BrCl-L}_1)\text{Cl}$, 2.3% in cells exposed to $\text{Cu}(\text{Cl}_2\text{-L}_1)\text{NO}_3$ compared to 0.4% in DMSO control) (Fig. 10). Interestingly, exposure of A2780 cells to IC_{50} concentration of $\text{Cu}(\text{BrCl-L}_1)\text{Cl}$ also displayed a very high increase in cells in early apoptosis when compared to the DMSO control (15.2% versus 2.2%) (Fig. 10). Interestingly, in the presence of complex $\text{Cu}(\text{BrCl-L}_1)\text{Cl}$ the number of cells in apoptosis is even higher than that for cisplatin (38.9% versus 14.2%, respectively). None of the complexes were able to induce necrosis (Fig. 10). Complex $\text{Cu}(\text{Cl}_2\text{-L}_1)\text{Cl}$ induced the lowest levels of apoptosis, 2.7% of early and 0.6% of late apoptosis when com-

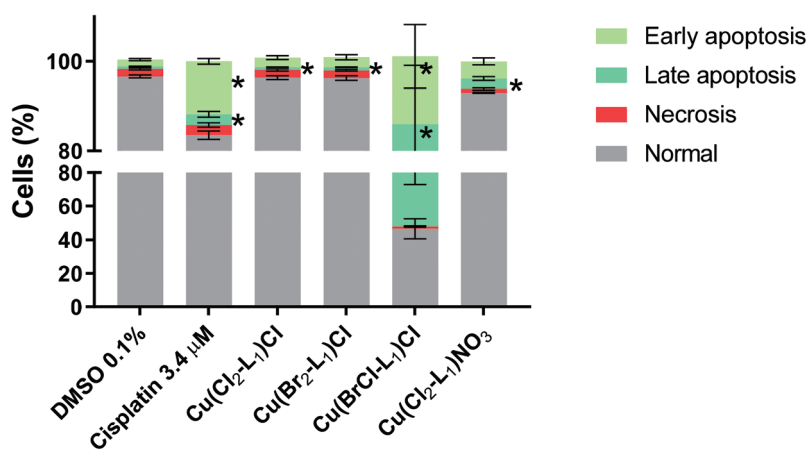


Fig. 10 Cell death mechanism induced in A2780 cells after 48 h exposure to the IC_{50} concentrations of $\text{Cu}(\text{Cl}_2\text{-L}_1)\text{Cl}$, $\text{Cu}(\text{Br}_2\text{-L}_1)\text{Cl}$, $\text{Cu}(\text{BrCl-L}_1)\text{Cl}$ and $\text{Cu}(\text{Cl}_2\text{-L}_1)\text{NO}_3$ evaluated by flow cytometry. DMSO 0.1% (v/v) was used as solvent control and cisplatin (3.4 μM ; IC_{50}) was used as a positive control. The results are expressed as the mean \pm SD from three independent assays. The symbol * indicates a p -value < 0.05 .

pared to the DMSO control, 2.2% and 0.4%, respectively, despite with statistical significance (Fig. 10) indicating that other types of cell death might be involved in the loss of cell viability.

To further confirm the higher induction of apoptosis in A2780 cells exposed to $\text{Cu}(\text{BrCl-L}_1)\text{Cl}$, the mitochondrial membrane potential was analysed using the JC-1 monomer/aggregate ratio (Fig. 11). JC-1 is a monomeric fluorescent dye that aggregates when in contact with the normal mitochondrial membrane potential.⁴³ The aggregation of the dye causes a redshift in the emission spectrum.⁴³ By measuring the green and red fluorescence it is possible to obtain a monomer/aggregate ratio. Normalizing the ratio for the vehicle control, DMSO 0.1% (v/v) it is possible to observe a hyperpolarization of the mitochondrial membrane when the monomer/aggregate ratio is <1 and a depolarization of the mitochondrial membrane when the monomer/aggregate ratio is >1 (Fig. 11).

The results indicate that exposure of A2780 cells to $\text{Cu}(\text{BrCl-L}_1)\text{Cl}$ promotes a depolarization of the mitochondrial membrane potential, at levels similar to cisplatin (Fig. 11). Depolarization of mitochondrial membrane potential is an early event in the induction of apoptosis through intracellular signalling, the intrinsic pathway.⁴⁴ These results indicate that $\text{Cu}(\text{BrCl-L}_1)\text{Cl}$ cytotoxicity may be due to induction of intrinsic apoptosis in the A2780 ovarian cancer cell line (Fig. 11).

Considering that for $\text{Cu}(\text{Cl}_2\text{-L}_1)\text{Cl}$ and $\text{Cu}(\text{Br}_2\text{-L}_1)\text{Cl}$ complexes a lower level of apoptosis was triggered (Fig. 10); another type of cell death mechanism – autophagy – was studied for all complexes (Fig. 12).

When compared to A2780 cells exposed to the DMSO 0.1% (v/v) control, all complexes were able to trigger autophagy

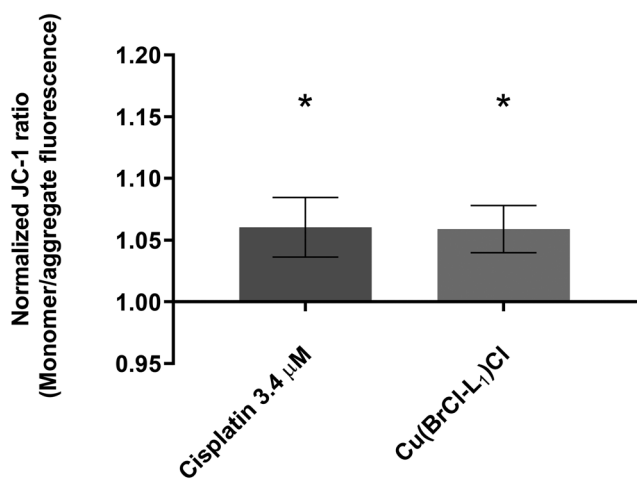


Fig. 11 Normalized mitochondrial membrane potential ratios of A2780 cells incubated for 48 h with cisplatin 3.4 μM (positive control) and with 16.5 μM (IC_{50} concentration) of $\text{Cu}(\text{BrCl-L}_1)\text{Cl}$ determined by flow cytometry using JC-1 dye. Ratios were normalized with the vehicle control DMSO 0.1% (v/v). The fluorescence was measured by flow cytometry in BL1 (530/30 nm) and BL2 (574/26 nm) channels. The results are expressed as the mean \pm SD from three independent assays. The symbol * indicates a p -value <0.05 .

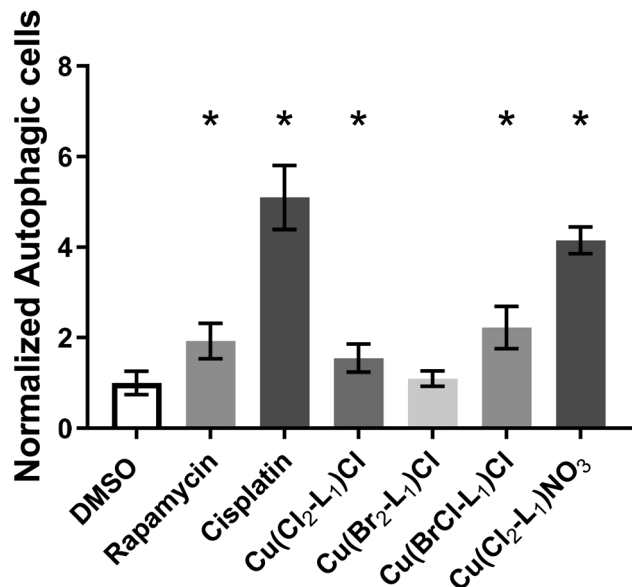


Fig. 12 Induction of autophagy in the A2780 cell line by flow cytometry. Cells were exposed to IC_{50} concentrations of $\text{Cu}(\text{Cl}_2\text{-L}_1)\text{Cl}$, $\text{Cu}(\text{Br}_2\text{-L}_1)\text{Cl}$, $\text{Cu}(\text{BrCl-L}_1)\text{Cl}$ and $\text{Cu}(\text{Cl}_2\text{-L}_1)\text{NO}_3$ for 48 h. Controls were performed with cells treated with DMSO 0.1% (v/v), vehicle control, and Rapamycin 0.02 μM as autophagy positive control. Cisplatin 3.4 μM, was also used as a positive control. Results were normalized to the DMSO 0.1% control and expressed as the mean \pm SD from three independent assays. The symbol * indicates a p -value <0.05 .

(Fig. 12). However, this effect was much more pronounced for $\text{Cu}(\text{BrCl-L}_1)\text{Cl}$, $\text{Cu}(\text{Cl}_2\text{-L}_1)\text{NO}_3$ and cisplatin, respectively, with 2.2 \times , 4.2 \times and 5.5 \times more autophagic cells in A2780 exposed for 48 h compared to the control (Fig. 12). This result indicates that for all complexes but particularly, for $\text{Cu}(\text{BrCl-L}_1)\text{Cl}$ and $\text{Cu}(\text{Cl}_2\text{-L}_1)\text{NO}_3$ the loss of cell viability is due to the induction of both apoptosis and autophagy. What is more, results of cell viability (IC_{50}) correlate with the autophagic potential particularly for $\text{Cu}(\text{Cl}_2\text{-L}_1)\text{NO}_3$ and cisplatin in the order cisplatin $>$ $\text{Cu}(\text{Cl}_2\text{-L}_1)\text{NO}_3 \gg \text{Cu}(\text{Cl}_2\text{-L}_1)\text{Cl}$, $\text{Cu}(\text{Br}_2\text{-L}_1)\text{Cl}$ and $\text{Cu}(\text{BrCl-L}_1)\text{Cl}$.

Mitochondria are the main site for reactive oxygen species (ROS) formation. An increase in the levels of ROS has been described and correlated with the induction of programmed cell death in eukaryotic cells.^{44,45} Thus, an evaluation of intracellular ROS production was performed in A2780 cells exposed to IC_{50} concentrations of the complexes $\text{Cu}(\text{Cl}_2\text{-L}_1)\text{Cl}$, $\text{Cu}(\text{Br}_2\text{-L}_1)\text{Cl}$, $\text{Cu}(\text{BrCl-L}_1)\text{Cl}$ and $\text{Cu}(\text{Cl}_2\text{-L}_1)\text{NO}_3$ (Fig. 13).

The exposure of A2780 cells to the IC_{50} concentrations of $\text{Cu}(\text{Cl}_2\text{-L}_1)\text{Cl}$, $\text{Cu}(\text{Br}_2\text{-L}_1)\text{Cl}$, $\text{Cu}(\text{BrCl-L}_1)\text{Cl}$ and $\text{Cu}(\text{Cl}_2\text{-L}_1)\text{NO}_3$ revealed that intracellular ROS were, respectively, 1.3 \times , 1.2 \times , 1.5 \times and 2.4 \times higher, with statistical significance, compared to A2780 cells exposed to DMSO 0.1% (v/v), (Fig. 13). Our results seem to point that the increase in intracellular ROS plays an important role in the cytotoxicity of $\text{Cu}(\text{Cl}_2\text{-L}_1)\text{Cl}$, $\text{Cu}(\text{Br}_2\text{-L}_1)\text{Cl}$, $\text{Cu}(\text{BrCl-L}_1)\text{Cl}$ and $\text{Cu}(\text{Cl}_2\text{-L}_1)\text{NO}_3$ in the A2780 cell line (Fig. 13) and might be correlated with the loss of cell viability (Fig. 8) and induction of cell death *via* apoptosis and autophagy (Fig. 10–12). Once again the higher loss of cell viability

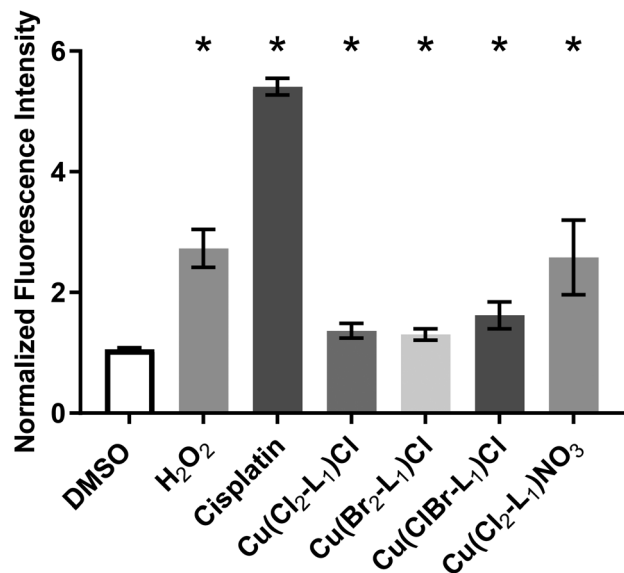


Fig. 13 Reactive oxygen species (ROS) induced by 48 h exposure of A2780 cells to IC₅₀ concentrations of Cu(Cl₂-L₁)Cl, Cu(Br₂-L₁)Cl, Cu(BrCl-L₁)Cl and Cu(Cl₂-L₁)NO₃ evaluated by flow cytometry. DMSO 0.1% (v/v) was used as the solvent control and H₂O₂ 25 μM and cisplatin 3.4 μM were used as positive controls. The results are expressed as the mean ± SD from three independent assays. The symbol * indicates a *p*-value < 0.05.

(lower IC₅₀) (Table 5) is observed for cisplatin and Cu(Cl₂-L₁)NO₃ in agreement with the higher ROS induction (Fig. 13) triggering a higher cell death (autophagy) (Fig. 12).

To better explain these results, we have assessed the internalization of complexes by measuring intracellular Cu by ICP-AES in A2780 cells exposed to the IC₅₀ of each complex (Fig. 14). Since copper is an essential metal present within our cells, results were normalized by the amount of Cu within cells not exposed to the Cu(II) complexes. Interestingly, when we compare the % of intracellular Cu after exposure of cells to Cu(Cl₂-L₁)NO₃ or Cu(Cl₂-L₂)NO₃ it is clear that there is an increased internalization of complex with the L₁ ligand compared to complex with the L₂ ligand (Fig. 14) that might correlate with its higher cytotoxicity towards A2780 cells (Table 5 and Fig. 8). Moreover, when we compare the four complexes with the L₁ ligand, Cu(Cl₂-L₁)NO₃, Cu(BrCl-L₁)Cl, Cu(Cl₂-L₁)Cl and Cu(Br₂-L₁)Cl, the % of intracellular Cu follows the intracellular ROS levels and autophagic cell death, with Cu(Cl₂-L₁)NO₃ > Cu(BrCl-L₁)Cl > Cu(Cl₂-L₁)Cl > Cu(Br₂-L₁)Cl, (Fig. 13 and 12, respectively).

Taken together, our results show that 48 h of exposure to the IC₅₀ concentration of Cu(BrCl-L₁)Cl in the A2780 cell line leads to the induction of intracellular ROS which trigger the induction of apoptosis, *via* the depolarization of the mitochondrial membrane and autophagy (Fig. 10–13). For complex Cu(Cl₂-L₁)NO₃ the same effect is observed but autophagy seems to be the preferable mechanism of cell death triggered by complex exposure (Fig. 10–13). Also the % of intracellular Cu correlates with the induction of higher cytotoxicity levels for

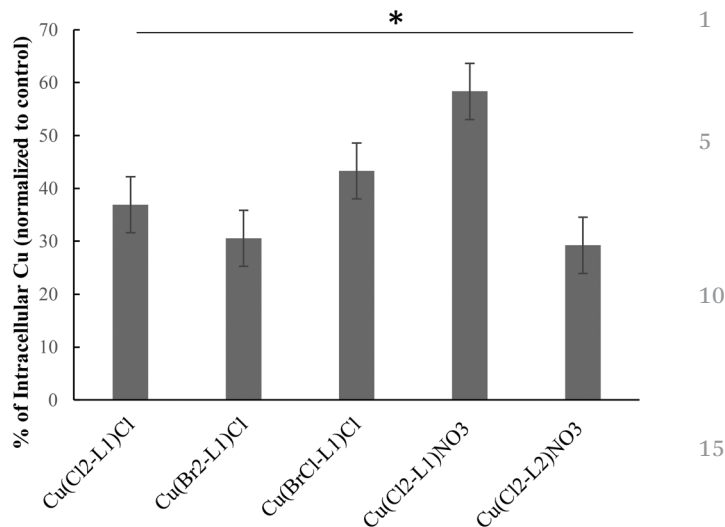


Fig. 14 Accumulation of complexes in the cellular fraction as evaluated by ICP-AES determination of Cu in the cellular fractions of A2780 ovarian cancer cultures after by 3 h exposure to the respective IC₅₀ of the complexes. The results presented are average (normalized to control) ± SD of three independent assays. The symbol * indicates a *p*-value < 0.05.

Cu(Cl₂-L₁)NO₃ and high intracellular ROS and cell death (Fig. 8 and 12–14). Higher levels of intracellular ROS have been described as either a consequence of or a trigger of different types of cell death.^{46–49} However, in A2780 cells exposed to Cu(Cl₂-L₁)Cl, only a small increase in autophagy was observed (1.4× higher compared to DMSO control) (Fig. 12). Similarly, A2780 cell line exposure to Cu(Br₂-L₁)Cl led to a statistically significant but small increase of late apoptosis, 0.7% when compared to 0.4% of late apoptotic cells observed in the DMSO control (Fig. 10).

To try to add more insights into the differences in apoptosis and autophagy observed for Cu(Cl₂-L₁)Cl and Cu(Br₂-L₁)Cl complexes, A2780 cells were exposed for 48 h to 0.1× IC₅₀, IC₅₀ and 10× IC₅₀ concentrations of complexes Cu(Cl₂-L₁)Cl and Cu(Br₂-L₁)Cl and cell death was evaluated with the trypan blue exclusion method (Fig. 15 and Fig. S3†). Trypan blue is a vital dye impermeable to viable cells and stains cells with a compromised plasma membrane (dead cells will become blue).⁵⁰ Using the trypan blue method, we are able to stain not only the adherent cells but also cells in the supernatant (detached from the bottom of the culture wells) and scored them as live or dead (Fig. 15 and S3†). Results presented in Fig. 15 are represented as percentage of cells and in ESI Fig. S3† as the total number of cells.

It is possible to observe that a concentration of 0.1 × IC₅₀ of complexes Cu(Cl₂-L₁)Cl and Cu(Br₂-L₁)Cl induces an increase of adherent dead cells (Fig. 15A and Fig. S3A†). When the concentrations of complexes Cu(Cl₂-L₁)Cl and Cu(Br₂-L₁)Cl raise to the IC₅₀, there is an increase of both living and dead cells in the culture media supernatant, which indicates a detachment of cells from the surface of the culture wells (Fig. 15B and Fig. S3B†).

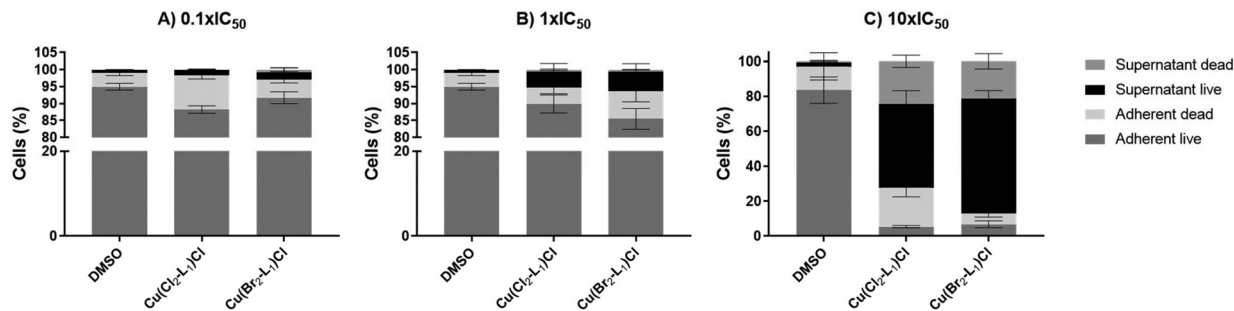


Fig. 15 Evaluation by the trypan blue exclusion method of the percentage of live and dead cells in the population of adherent and in the culture media supernatant (non-adherent) A2480 cells. Cells were incubated for 48 h with DMSO 0.01% (v/v) (A), DMSO 0.1% (v/v) (B) and DMSO 1% (C) as solvent controls and with $0.1 \times IC_{50}$ (A), $1 \times IC_{50}$ (B) and $10 \times IC_{50}$ (C) concentrations of complexes $Cu(Cl_2-L_1)Cl$ and $Cu(Br_2-L_1)Cl$. The results shown are expressed as the mean \pm SD from three independent assays.

This detachment of cells is dependent on the concentration of complexes, since both the percentage and number of cells in the supernatant increase when the concentration of complexes is raised to $10 \times IC_{50}$ (Fig. 15C and Fig. S3C†). Therefore, incubation with complexes $Cu(Cl_2-L_1)Cl$ and $Cu(Br_2-L_1)Cl$ leads to A2780 cellular detachment from culture plates (Fig. 15 and Fig. S3†). These results may shed some light into the reason why a low level of apoptosis or even autophagy was detected in A2780 exposed to the IC_{50} concentrations of complexes $Cu(Cl_2-L_1)Cl$ and $Cu(Br_2-L_1)Cl$ (Fig. 10 and 13). The methods used for the detection of both types of cell death rely on protocols designed to test adherent cells and not cells in the culture medium (supernatant), meaning that an underestimation of apoptosis and autophagy through analysis by flow cytometry might occur.

Comparing our cytotoxicity results with similar complexes described in the literature is not an easy task since different methodologies (e.g. different cell lines used and time points) are used. However, a comparison might be made with results of Maheswari *et al.*, 2006 where the authors used Cu(II) complexes with Schiff-base ligands that include substituted salicylaldehyde, Hpyrimol, salicylaldehyde semicarbazone and salicylaldehyde hydrazone ligands. In this work the authors report an IC_{50} value of $3.4 \mu M$ in the A2780 cancer cell line for a Cu(II) complex with a Hpyrimol ligand, $3 \times$ lower than the complexes here described.¹⁹ Other studies report IC_{50} values ranging from 1 to $55 \mu M$ in different cell lines that include A2780, MCF7, MOLT-4, A549, SK-II, HCT8, ME180 and L1210.^{19,20,51–55} These Cu(II) complexes have also been described to trigger apoptosis which is in line with the results indicated in the present work.^{19,20,52–56}

Conclusion

To investigate the effect of different halogen substituents, leaving groups and flexibility of ligands on the anticancer activity of copper complexes, a series of copper(II) complexes containing tridentate Schiff-base ligands have been prepared and characterized by several spectroscopic methods, and some

of them by X-ray crystallography. *In vitro* cytotoxicity assay revealed an antiproliferative activity of $Cu(Cl_2-L_1)Cl$, $Cu(Br_2-L_1)Cl$, $Cu(BrCl-L_1)Cl$ and $Cu(Cl_2-L_1)NO_3$ towards the A2780 ovarian carcinoma cell line compared to the other tumor cell lines studied (HCT116 and MCF7). Complex $Cu(Cl_2-L_1)NO_3$ demonstrated a higher selectivity index towards A2780 cells compared to normal fibroblasts. Interestingly, when we compared internalization of $Cu(Cl_2-L_1)NO_3$ and $Cu(Cl_2-L_2)NO_3$ clearly the amount of intracellular Cu correlates with cytotoxicity ($Cu(Cl_2-L_1)NO_3 \gg Cu(Cl_2-L_2)NO_3$). Moreover, the % of internalized Cu was higher for $Cu(Cl_2-L_1)NO_3$ compared with the other Cu(II) complexes with the L_1 ligand also agreeing with the cytotoxicity and higher selectivity towards A2780 cells.

Exposure of A2780 cells to the four complexes, $Cu(Cl_2-L_1)Cl$, $Cu(Br_2-L_1)Cl$, $Cu(BrCl-L_1)Cl$ and $Cu(Cl_2-L_1)NO_3$ leads to an increase in the intracellular ROS that could be related to the induced cell death and loss of cell viability. Indeed, the amount of Cu internalized due to the incubation of cells with the four complexes could be correlated with the level of intracellular ROS and trigger of cell death.

The $Cu(BrCl-L_1)Cl$ complex was able to trigger apoptosis *via* the intrinsic pathway, and also autophagy. Although the $Cu(Cl_2-L_1)NO_3$ complex also triggered both cell death mechanisms, a higher level of autophagy was induced. Incubation of A2780 cells with $Cu(Cl_2-L_1)Cl$ seemed to trigger cell death *via* autophagy and $Cu(Br_2-L_1)Cl$ triggered apoptosis. Nevertheless, $Cu(Cl_2-L_1)Cl$ and $Cu(Br_2-L_1)Cl$ complexes lead to cellular detachment, underestimating the number of cells measured by flow cytometry and allowing to correlate with the results of loss of cell viability. Cu(II) complexes with Schiff-base ligands have been previously reported to trigger apoptosis *in vitro* which supports our findings.

Experimental section

Chemicals and instrumentation

Copper(II) chloride, copper(II) nitrate, 3,5-dibromosalicylaldehyde, 3,5-diiodosalicylaldehyde, 3,5-dichlorosalicylaldehyde, 3-bromo-5-chlorosalicylaldehyde, salicylaldehyde, 2-(2-pyridyl)

ethylamine and 2-picoylamine were purchased from Sigma-Aldrich and used without further purification. The commercial solvents were distilled and then used for preparation of ligands and complexes. The FT-IR spectrum was recorded on a JASCO, FT/IR-6300 spectrometer (4000–400 cm^{-1}) in KBr pellets. The elemental analysis was performed on Leco, CHNS-932 and PerkinElmer 7300 DV elemental analyzers.

Biological assays

Cell culture. A2780 and HCT116 cancer derived cell lines (from human ovary and colorectal carcinomas, respectively) and normal human dermal fibroblasts were cultivated in RPMI 1640 medium (A2780) or in Dulbecco's modified Eagle's medium (DMEM) (HCT116 and fibroblasts). All culture media were supplemented with 1% (v/v) PenStrep solution and 10% (v/v) fetal bovine serum (FBS) (all from Thermo Fischer Scientific, Waltham, MA, USA). Cells were grown at 37 °C, under an atmosphere with high humidity and 5% (v/v) CO_2 , as described elsewhere. The A2780 cancer cell line was purchased from Merck (Darmstadt, Germany) and HCT116 cancer cell line and normal epidermal human fibroblasts from American Type Culture Collection (ATCC, Manassas, VA, USA).^{57–59}

Viability assays in A2780 and HCT116 cancer cell lines and in normal human dermal fibroblasts

Cells were seeded in 96 well-plates (7500 cells/100 μL well). After 24 h incubation, cells were incubated with DMSO (vehicle control), cisplatin (positive control) or increasing concentrations of the $\text{Cu}(\text{Cl}_2\text{-L}_1)\text{Cl}$, $\text{Cu}(\text{Br}_2\text{-L}_1)\text{Cl}$, $\text{Cu}(\text{BrCl-L}_1)\text{Cl}$ and $\text{Cu}(\text{Cl}_2\text{-L}_1)\text{NO}_3$ complexes. Cell cultures were then incubated for 48 h and cell viability was determined with the CellTiter 96® aqueous non-radioactive proliferation assay (MTS assay) (Promega, Madison, WI, USA).^{57,58} Dehydrogenases present in metabolically active cells reduce 3-(4,5-dimethylthiazol-2-yl)-5-(3-carboxymethoxyphenyl)-2-(4-sulphophenyl)-2H-tetrazolium, inner salt (MTS), producing formazan which can be measured at 490 nm in a Tecan microplate reader, Infinite M200 (Tecan, Männedorf, Switzerland). The amount of formazan is directly proportional to viable cells. The IC_{50} values are the concentrations that inhibit cellular proliferation by 50% compared to the vehicle control (DMSO 0.1% v/v). The IC_{50} values are used to compare the biological activity of the different complexes. IC_{50} values were determined with GraphPad Prism 8.2.1 software (GraphPad Software, La Jolla, CA, USA) through analysis of the dose response curves.

Apoptosis induction in the A2780 cell line

Annexin V-Alexafluor 488/PI dead cell apoptosis assay (ThermoFisher Scientific) was used to quantify apoptosis in A2780 cells by flow cytometry. Six well plates with A2780 cells (2×10^5 cells/1 mL well) were seeded and incubated for 24 h, and then incubated for 48 h with DMSO 0.1% (v/v), as the vehicle control, cisplatin 3.4 μM (positive control) and with IC_{50} concentrations of $\text{Cu}(\text{Cl}_2\text{-L}_1)\text{Cl}$, $\text{Cu}(\text{Br}_2\text{-L}_1)\text{Cl}$, $\text{Cu}(\text{BrCl-L}_1)\text{Cl}$ and $\text{Cu}(\text{Cl}_2\text{-L}_1)\text{NO}_3$ complexes. As the positive control, A2780 cells were also treated with cisplatin 3.4 μM . According

to the instructions of the manufacturer, cells were detached with trypsin and washed with PBS 1× before being incubated at room temperature for 15 minutes with Annexin V-Alexafluor 488 assay solution and 10 $\mu\text{g mL}^{-1}$ propidium iodide.^{43,57} Cells were analyzed in an Attune acoustic focusing cytometer (ThermoFisher Scientific) and results were analyzed with the respective software (Attune Cytometric Software, vs. 2.1).

Alterations of mitochondrial membrane potential

JC-1 dye, 5,5',6,6'-tetrachloro-1,1',3,3'-tetraethylbenzimidazolcarbocyanine iodide, (Abnova, Taipei, Taiwan) was used to evaluate alterations in the mitochondrial membrane potential.^{43,57} JC-1 is a green fluorescent dye in the monomeric form. However, when the dye is in contact with the intact electrochemical gradient of the mitochondrial membrane, it aggregates, which results in a redshift of the emission spectrum.^{43,57} As described above, 6-well plates with 2×10^5 A2780 cells per well were seeded and incubated for 24 h before being incubated with 0.1% (v/v) DMSO, cisplatin 3.4 μM and with IC_{50} concentration of the $\text{Cu}(\text{BrCl-L}_1)\text{Cl}$ complex. After 48 h incubation, JC-1 dye was added to the cells according to the manufacturer's instructions. An Attune focusing flow cytometer (ThermoFisher Scientific) was used to quantify the fluorescence of the monomer (BL-1 filter) and the aggregate (BL-2 filter) with the respective software (Attune Cytometric Software, vs. 2.1). The values obtained for DMSO treated cells were used to normalize the JC-1 ratios obtained for cisplatin 3.4 μM and $\text{Cu}(\text{BrCl-L}_1)\text{Cl}$.

Intracellular reactive oxygen species (ROS) production in the A2780 cell line

The method uses 2',7'-dichlorodihydrofluorescein diacetate dye (H2DCF-DA) (ThermoFisher Scientific) to detect intracellular ROS. Intracellular esterases remove acetate groups from this dye allowing to be reduced, which increases its fluorescence. In 6-well plates, 2×10^5 A2780 cells per well are incubated for 24h. Cells were then incubated with DMSO 0.1% (v/v) (vehicle control), 25 μM H_2O_2 and 3.4 μM cisplatin (positive controls) and IC_{50} concentrations of $\text{Cu}(\text{Cl}_2\text{-L}_1)\text{Cl}$, $\text{Cu}(\text{Br}_2\text{-L}_1)\text{Cl}$, $\text{Cu}(\text{BrCl-L}_1)\text{Cl}$ and $\text{Cu}(\text{Cl}_2\text{-L}_1)\text{NO}_3$ complexes for 48 h. Then an incubation of A2780 cancer cells with 10 μM H2DCF-DA (ThermoFisher Scientific) was performed for 30 min at 37 °C. Cells were then analyzed in an Attune acoustic focusing cytometer (ThermoFisher Scientific) and the experimental data were analyzed with the respective software (Attune Cytometric Software, vs. 2.1).^{43,57}

Autophagy induction in the A2780 cell line

An autophagy assay kit (Abcam) was used to detect A2780 cells in autophagy. A2780 cells were seeded in 6-well plates at a density of 2×10^5 cells per well and incubated for 24 h. Then, A2780 cells were incubated with DMSO 0.1% (v/v) and with rapamycin 0.2 μM (vehicle and positive control, respectively) and with IC_{50} concentrations of $\text{Cu}(\text{Cl}_2\text{-L}_1)\text{Cl}$, $\text{Cu}(\text{Br}_2\text{-L}_1)\text{Cl}$, $\text{Cu}(\text{BrCl-L}_1)\text{Cl}$ and $\text{Cu}(\text{Cl}_2\text{-L}_1)\text{NO}_3$ complexes for 48 h. According to the manufacturer's instructions, cells were detached with

trypsin and washed with reaction buffer 1×. Then an incubation of A 2780 cells with green stain solution was performed for 30 min at room temperature. Before analysis, cells were washed and then resuspended with reaction buffer 1×. The Attune acoustic focusing cytometer (ThermoFisher Scientific) and the respective software (Attune Cytometric Software, v8.2.1) were used to analyze cells.^{43,57}

Internalization of complexes in the A2780 cell line

ICP-AES, inductively coupled plasma atomic emission spectroscopy, was used to determine the amount of Cu in A2780 cells exposed to complexes $\text{Cu}(\text{Cl}_2\text{-L}_1)\text{Cl}$, $\text{Cu}(\text{Br}_2\text{-L}_1)\text{Cl}$, $\text{Cu}(\text{BrCl-L}_1)\text{Cl}$, $\text{Cu}(\text{Cl}_2\text{-L}_1)\text{NO}_3$ and $\text{Cu}(\text{Cl}_2\text{-L}_2)\text{NO}_3$. In 25 cm² T flasks, 5×10^6 cells were seeded and incubated for 24 h before culture media were removed and A2780 cells were incubated with the IC₅₀ concentrations of the above described complexes for 48 h, before the culture media were removed and washed twice with PBS. Vehicle control used was with DMSO 1%. The media and PBS were combined and treated with freshly made aqua regia (3 : 1 HCl : HNO₃). Cells were detached from the flasks with triple express (Thermo Fischer Scientific) and treated with fresh aqua regia. Pelleted cells formed the cellular fraction of the sample and culture media, and PBS from the wash, formed the extracellular fraction of the samples. Untreated A2780 cells were also prepared in the same way to provide the same biological matrix for Cu standards. Samples were incubated for 24 h in a hood fume at room temperature and delivered to Laboratório de Análises/LAUV were ICP-AES was performed. Results were shown as % of intracellular Cu (normalized to control cells) ± SD.

Cytotoxicity of the $\text{Cu}(\text{Cl}_2\text{-L}_1)\text{Cl}$ and $\text{Cu}(\text{Br}_2\text{-L}_1)\text{Cl}$ complexes in the A2780 cell line using the trypan blue exclusion method

Strober *et al.* described the trypan blue exclusion method.⁵⁰ The method relies on an exclusion dye, trypan blue, that cannot stain viable cells. Only dead cells will become blue due to the lack of a functional plasmatic membrane. A2780 cells were seed in 6-well plates (2×10^5 cells per well) and after an initial 24 h incubation, cells were incubated with 3 different concentrations of the vehicle control, DMSO (0.01%, 0.1% and 1% (v/v)) and of $\text{Cu}(\text{Cl}_2\text{-L}_1)\text{Cl}$ and $\text{Cu}(\text{Br}_2\text{-L}_1)\text{Cl}$ complexes (0.1 × IC₅₀, 1 × IC₅₀, and 10 × IC₅₀). After an incubation of 48 h, A2780 cells attached to the wells and cells in the culture medium supernatant were counted and the live and dead cells were scored. Cellular suspensions were mixed with trypan blue 0.4% (w/v) (ThermoFisher Scientific) in a 4 : 1 ratio (cells: trypan blue) as previously described.^{50,60} The cell suspensions were counted on a hemocytometer (Hirschmann, Eberstadt, Germany) with an inverted microscope Olympus CXX41 (Tokyo, Japan).

Statistical analysis

Results are presented throughout this manuscript as the mean ± SD of at least three independent experiments. The Student *t*-test was used to determine statistical significance. Results were considered statistically significant if $p < 0.05$. The

GraphPad Prism v8.2.1 program was used to perform statistical analysis (GraphPad Software, La Jolla, CA, USA).

Synthesis of the complexes

A general synthetic route was used for all complexes in which a solid sample of CuCl₂ or Cu(NO₃)₂ (1 mmol) was dissolved in 2 mL of MeOH and then 30 mL of MeOH solution containing the appropriate ligand (1 mmol) was added. The resulting solution was refluxed for 2 h.

$\text{Cu}(\text{Br}_2\text{-L}_1)\text{Cl}$: After addition of CuCl₂ to a solution of ligand, a green precipitate was formed. This green precipitate was collected by filtration, washed with cold methanol and dried in air. Yield: 86%. Anal. Calcd for C₁₃H₉Br₂ClCuN₂O: C, 33.36; H, 1.94; N, 5.99%. Found: C, 33.38; H, 1.92; N, 5.95%. Selected IR data (KBr, cm⁻¹): 3433 (m), 2921 (w), 1623 (s, C=N), 1440 (m), 1413 (m), 1316 (w), 1280 (w), 1155 (m), 1051 (w), 859 (w), 716 (m).

$\text{Cu}(\text{Cl}_2\text{-L}_1)\text{Cl}$: After addition of CuCl₂ to a solution of ligand, a green precipitate was formed. This green precipitate was collected by filtration, washed with cold methanol and dried in air. Yield: 90%. Anal. Calcd for C₁₃H₉Cl₃CuN₂O: C, 41.19; H, 2.39; N, 7.39%. Found: C, 41.25; H, 2.36; N, 7.42%. Selected IR data (KBr, cm⁻¹): 3433 (m), 3071 (w), 2924 (w), 1636 (s, C=N), 1519 (w), 1449 (m), 1285 (w), 1214 (w), 1168 (m), 1023 (w), 765 (m), 580 (w).

$\text{Cu}(\text{I}_2\text{-L}_1)\text{Cl}$: After addition of CuCl₂ to a solution of ligand, a green precipitate was formed. This green precipitate was collected by filtration, washed with cold methanol and dried in air. Yield: 93%. Anal. Calcd for C₁₃H₉ClCuI₂N₂O: C, 27.78; H, 1.61; N, 4.98%. Found: C, 27.73; H, 1.65; N, 5.02%. Selected IR data (KBr, cm⁻¹): 3432 (w), 3053 (m), 1619 (s, C=N), 1570 (w), 1485 (w), 1432 (w), 1409 (m), 1312 (w), 1218 (w), 1149 (m), 1052 (w), 995 (w), 824 (w), 759 (w), 464 (w).

$\text{Cu}(\text{BrCl-L}_1)\text{Cl}$: After addition of CuCl₂ to a solution of ligand, a green precipitate was formed. This green precipitate was collected by filtration, washed with cold methanol and dried in air. Yield: 89%. Anal. Calcd for C₁₃H₉BrCl₂CuN₂O: C, 36.86; H, 2.14; N, 6.61%. Found: C, 36.84; H, 2.16; N, 6.64%. Selected IR data (KBr, cm⁻¹): 3434 (m), 3059 (w), 2916 (w), 1624 (s, C=N), 1509 (w), 1441 (m), 1416 (m), 1211 (w), 1159 (m), 1051 (w), 860 (w), 750 (m), 584 (w), 470 (w).

$\text{Cu}(\text{Br}_2\text{-L}_1)\text{NO}_3$: After addition of Cu(NO₃)₂ to a solution of ligand, a green precipitate was quickly formed. The precipitate was collected by filtration, washed with cold methanol and dried in air. Yield: 92%. Anal. Calcd for C₁₃H₉Br₂CuN₃O₄: C, 31.57; H, 1.83; N, 8.50%. Found: C, 31.62; H, 1.53; N, 8.45%. Selected IR data (KBr, cm⁻¹): 3433 (m), 3060 (w), 2920 (w), 1629 (s, C=N), 1507 (w), 1471 (s), 1422 (s), 1289 (s), 1215 (w), 1153 (m), 1013 (m), 762 (w), 713 (w), 586 (w), 475 (w).

$\text{Cu}(\text{Cl}_2\text{-L}_1)\text{NO}_3$: After addition of Cu(NO₃)₂ to a methanolic solution of ligand, the color immediately changes from yellowish to green without any precipitation. The resulting solution was refluxed for about 2 h. The solution was allowed to stand at room temperature. The dark green precipitate was obtained at room temperature by slow evaporation of the solvent. Yield: 87%. Anal. Calcd for C₁₃H₉Cl₂CuN₃O₄: C, 38.49; H, 2.24; N,

10.36%. Found: C, 38.51; H, 2.20; N, 10.38%. Selected IR data (KBr, cm^{-1}): 3432 (m), 3068 (w), 2928 (w), 1631 (s, C=N), 1518 (w), 1473 (s), 1444 (s), 1290 (s), 1164 (m), 1051 (w), 1014 (m), 866 (w), 762 (m), 591 (w).

Cu(I₂L₁)NO₃: After addition of Cu(NO₃)₂ to a solution of ligand, a green precipitate was quickly formed. The precipitate was collected by filtration, washed with cold methanol and dried in air. Yield: 91%. Anal. Calcd for C₁₃H₉I₂CuN₃O₄: C, 26.53; H, 1.54; N, 7.14%. Found: C, 26.49; H, 1.68; N, 7.09%. Selected IR data (KBr, cm^{-1}): 3433 (m), 3046 (w), 1629 (s, C=N), 1570 (m), 1471 (s), 1319 (w), 1285 (s), 1149 (m), 1009 (m), 871 (w), 696 (w), 582 (w).

Cu(BrCl-L₁)NO₃: After addition of Cu(NO₃)₂ to a methanolic solution of ligand, the color immediately changes from yellowish to green without any precipitation. The resulting solution was refluxed about 2 h. The solution was allowed to stand at room temperature. The dark green precipitate was obtained at room temperature by slow evaporation of the solvent. Yield: 87%. Anal. Calcd for C₁₃H₉BrClCuN₃O₄: C, 34.69; H, 2.02; N, 9.34%. Found: C, 34.81; H, 1.93; N, 10.03%. Selected IR data (KBr, cm^{-1}): 3433 (m), 2925 (w), 1631 (s, C=N), 1511 (w), 1473 (s), 1442 (m), 1291 (s), 1212 (w), 1157 (m), 1015 (w), 866 (w), 749 (m), 470 (w).

Cu(Br₂L₂)Cl: After addition of Cu(NO₃)₂ to a methanolic solution of ligand, the color of the solution changed from yellow to dark green without any precipitation. The resulting solution was refluxed for about 2 h. The solution was allowed to stand at room temperature. The dark green precipitate was obtained at room temperature by slow evaporation of the solvent. Yield: 87%. Anal. Calcd for C₁₄H₁₁Br₂ClCuN₂O: C, 34.88; H, 2.30; N, 5.81%. Found: C, 34.81; H, 2.35; N, 5.78%. Selected IR data (KBr, cm^{-1}): 3433 (m), 2913 (w), 1625 (s, C=N), 1448 (s), 1214 (w), 1153 (m), 871 (w), 775 (w).

Cu(Cl₂L₂)Cl: After addition of Cu(NO₃)₂ to a methanolic solution of ligand, the color of the solution changed from yellow to dark green without any precipitation. The resulting solution was refluxed for about 2 h. The solution was allowed to stand at room temperature. The dark green precipitate was obtained at room temperature by slow evaporation of the solvent. Yield: 88%. Anal. Calcd for C₁₄H₁₁Cl₃CuN₂O: C, 42.77; H, 2.82; N, 7.13%. Found: C, 42.71; H, 2.97; N, 7.08%. Selected IR data (KBr, cm^{-1}): 3433 (m), 3056 (w), 2912 (w), 1620 (s, C=N), 1516 (w), 1435 (s), 1323 (w), 1166 (m), 961 (w), 867 (w), 759 (s), 584 (w), 538 (w).

Cu(I₂L₂)Cl: After addition of CuCl₂ to a solution of ligand, a green precipitate was formed. The precipitate was collected by filtration, washed with cold methanol and dried in air. Green crystals were formed from a methanolic solution of the complex by slow evaporation of the solvent after standing for one week in air. Yield: 79%. Anal. Calcd for C₁₄H₁₁ClCuI₂N₂O: C, 29.19; H, 1.92; N, 4.86%. Found: C, 29.28; H, 1.83; N, 4.91%. Selected IR data (KBr, cm^{-1}): 3433 (s), 2920 (w), 1610 (s, C=N), 1484 (w), 1430 (s), 1146 (s), 857 (w), 763 (m), 585 (w).

Cu(BrCl-L₂)Cl: After addition of Cu(NO₃)₂ to a methanolic solution of ligand, the color of the solution changed from yellow to dark green without any precipitation. The resulting

solution was refluxed for about 2 h. The solution was allowed to stand at room temperature. The dark green precipitate was obtained at room temperature by slow evaporation of the solvent. Yield: 81%. Anal. Calcd for C₁₄H₁₁BrCl₂CuN₂O: C, 38.43; H, 2.53; N, 6.40%. Found: C, 38.51; H, 2.49; N, 6.45%. Selected IR data (KBr, cm^{-1}): 3433 (s), 2914 (w), 1620 (s, C=N), 1479 (w), 1429 (s), 1411 (m), 1319 (w), 1207 (m), 869 (w), 737 (m).

Cu(Br₂L₂)NO₃: After addition of Cu(NO₃)₂ to a methanolic solution of ligand, the color of the solution changed from yellow to dark green without any precipitation. The resulting solution was refluxed for about 2 h. The solution was allowed to stand at room temperature. The dark green crystals were obtained at room temperature by slow evaporation of the solvent. Yield: 87%. Anal. Calcd for C₁₄H₁₁Br₂CuN₃O₄: C, 33.06; H, 2.18; N, 8.26%. Found: C, 33.17; H, 2.21; N, 8.34%. Selected IR data (KBr, cm^{-1}): 3434 (m), 3054 (w), 2957 (w), 1623 (m, C=N), 1381 (s), 1280 (w), 1155 (w), 959 (w), 866 (w), 758 (m), 584 (w).

Cu(Cl₂L₂)NO₃: After addition of Cu(NO₃)₂ to a methanolic solution of ligand, the color of the solution changed from yellow to dark green without any precipitation. The resulting solution was refluxed for about 2 h. The solution was allowed to stand at room temperature. The dark green crystals were obtained at room temperature by slow evaporation of the solvent. Yield: 82%. Anal. Calcd for C₁₄H₁₁Cl₂CuN₃O₄: C, 40.06; H, 2.64; N, 10.01%. Found: C, 40.19; H, 2.73; N, 9.1%. Selected IR data (KBr, cm^{-1}): 3434 (s), 2921 (w), 1631 (s, C=N), 1445 (m), 1380 (m), 1210 (w), 1164 (m), 1014 (w), 763 (m), 591 (w).

Cu(I₂L₂)NO₃: After addition of Cu(NO₃)₂ to a methanolic solution of ligand, the color of the solution changed from yellow to dark green without any precipitation. The resulting solution was refluxed for about 2 h. The solution was allowed to stand at room temperature. The dark green precipitate was obtained at room temperature by slow evaporation of the solvent. Yield: 91%. Anal. Calcd for C₁₄H₁₁CuI₂N₃O₄: C, 27.90; H, 1.84; N, 6.97%. Found: C, 27.90; H, 1.84; N, 7.11%. Selected IR data (KBr, cm^{-1}): 3409 (m), 1627 (s, C=N), 1383 (s), 1282 (w), 1166 (w), 761 (m).

Cu(BrCl-L₂)NO₃: After addition of Cu(NO₃)₂ to a methanolic solution of ligand, the color of the solution changed from red to dark green without any precipitation. The resulting solution was refluxed for about 2 h. The solution was allowed to stand at room temperature. The dark green crystals were obtained at room temperature by slow evaporation of the solvent. Yield: 89%. Anal. Calcd for C₁₄H₁₁BrClCuN₃O₄: C, 36.23; H, 2.39; N, 9.05%. Found: C, 36.36; H, 2.32; N, 8.84%. Selected IR data (KBr, cm^{-1}): 3432 (m), 3067 (w), 2922 (w), 1625 (s, C=N), 1447 (s), 1383 (w), 1283 (s), 1210 (w), 1160 (m), 1007 (w), 866 (w), 748 (m).

X-ray crystal structure determination

The diffraction data (except compound Cu(BrCl-L₂)NO₃) were measured at low temperature using Cu or Mo K_α radiation on a Rigaku SuperNova dual system in combination with an Atlas

1 type CCD detector. The data reduction was carried out using
 CrysAlis^{Pro}.⁶¹ The data for crystal structure **Cu(BrCl-L₂)NO₃**,
 were collected at 120 K using Mo K α radiation on a Bruker
 APEX II CCD diffractometer equipped with a kappa geometry
 5 goniometer. The dataset was reduced using EvalCCD⁶² and
 then corrected for absorption.⁶³

The solution analysis and refinements were performed
 using SHELXT⁶⁴ and SHELXL,⁶⁵ respectively. The crystal struc-
 10 tures were refined using full-matrix least-squares based on F^2
 with all non-hydrogen atoms anisotropically defined.
 Hydrogen atoms were placed in calculated positions by means
 of the “riding” model. Pseudo merohedral twinning was found
 for all crystal structures and treated directly with CrysAlis^{Pro}⁶¹
 15 or with the TWINROT/MAT routine of PLATON.⁶⁶ Constraints
 and rigid bond restraints (EADP and RIGU cards) were
 employed during the last stages of refinement of **Cu(BrCl-L₂)**
NO₃ in order to obtain acceptable anisotropic displacement
 parameters. More details concerning the crystal structures and
 20 their refinement can be found in Table 3 or in the corres-
 ponding CIFs.

In particular, for compound **Cu(BrCl-L₁)NO₃**, the obtained
 twin law is $-1\ 0\ 0\ 0\ -1\ 0\ 0.082\ 0\ 1$ and the BASF parameter is
 0.123(1). Applying the twin improved the refinement by about
 25 4.5% and reduced the residual electron densities by about 2.
 Nevertheless, some relatively high peaks still reside close to
 heavy atoms (Br, Cu) and this could be likely due to absorption
 effects.

Conflicts of interest

The authors declare no competing financial interest.

Acknowledgements

The authors are grateful to the Research Council of the
 40 University of Isfahan for financial support of this work. This
 work was supported by the Applied Molecular Biosciences
 Unit-UCIBIO which is financed by national funds from FCT/
 MCTES (UIDB/04378/2020).

References

Q7

- 1 M. Gielen and E. R. Tiekink, John Wiley & Sons, 2005.
- 2 S. Dhar, D. Senapati, P. K. Das, P. Chattopadhyay,
 M. Nethaji and A. R. Chakravarty, *J. Am. Chem. Soc.*, 2003,
 40 **40**, 12118–12124.
- 3 L. Kelland, *Nat. Rev. Cancer*, 2007, **8**, 573.
- 4 L. Kelland, *Expert Opin. Invest. Drugs*, 2007, **7**, 1009–1021.
- 5 M. Galanski, V. Arion, M. Jakupec and B. Keppler, *Curr.*
 55 *Pharm. Des.*, 2003, **25**, 2078–2089.
- 6 D. Wang and S. J. Lippard, *Nat. Rev. Drug Discovery*, 2005, **4**,
 307.

- 7 A. M. Angeles-Boza, P. M. Bradley, P. K.-L. Fu, S. E. Wicke,
 J. Bacsá, K. R. Dunbar and C. Turro, *Inorg. Chem.*, 2004, **26**,
 8510–8519.
- 8 C. A. Rabik and M. E. Dolan, *Cancer Treat. Rev.*, 2007, **1**, 9–23.
- 9 K. R. G. Knight, D. F. Kraemer and E. A. Neuwelt, *J. Clin.*
 5 *Oncol.*, 2005, **34**, 8588–8596.
- 10 Y. An, S.-D. Liu, S.-Y. Deng, L.-N. Ji and Z.-W. Mao, *J. Inorg.*
Biochem., 2006, **10**, 1586–1593.
- 11 S. Zhang, C. Tu, X. Wang, Z. Yang, J. Zhang, L. Lin, J. Ding
 and Z. Guo, *Eur. J. Inorg. Chem.*, 2004, **20**, 4028–4035.
- 12 R. S. Kumar, K. Sasikala and S. Arunachalam, *J. Inorg.*
Biochem., 2008, **2**, 234–241.
- 13 S. Dhar and A. R. Chakravarty, *Inorg. Chem.*, 2003, **8**, 2483–
 2485.
- 14 G. L. Eichhorn and Y. A. Shin, *J. Am. Chem. Soc.*, 1968, **26**,
 7323–7328.
- 15 C. Santini, M. Pellei, V. Gandin, M. Porchia, F. Tisato and
 C. Marzano, *Chem. Rev.*, 2013, **1**, 815–862.
- 16 K. G. Daniel, D. Chen, S. Orlu, Q. C. Cui, F. R. Miller and
 20 Q. P. Dou, *Breast Cancer Res.*, 2005, **6**, R897.
- 17 K. G. Daniel, P. Gupta, R. H. Harbach, W. C. Guida and
 Q. P. Dou, *Biochem. Pharmacol.*, 2004, **6**, 1139–1151.
- 18 D. Chen and Q. P. Dou, *Expert Opin. Ther. Targets*, 2008, **6**,
 739–748.
- 19 P. U. Maheswari, S. Roy, H. den Dulk, S. Barends, G. van
 25 Wezel, B. Kozlevcar, P. Gamez and J. Reedijk, *J. Am. Chem.*
Soc., 2006, **3**, 710–711.
- 20 V. Rajendiran, R. Karthik, M. Palaniandavar, H. Stoeckli-
 Evans, V. S. Periasamy, M. A. Akbarsha, B. S. Srinag and
 H. Krishnamurthy, *Inorg. Chem.*, 2007, **20**, 8208–8221.
- 21 Y. Lu, Y. Wang and W. Zhu, *Phys. Chem.*, 2010, **18**, 4543–4551.
- 22 E. Parisini, P. Metrangolo, T. Pilati, G. Resnati and
 G. Terraneo, *Chem. Soc. Rev.*, 2011, **5**, 2267–2278.
- 23 L. A. Hardegger, B. Kuhn, B. Spinnler, L. Anselm,
 30 R. Ecabert, M. Stihle, B. Gsell, R. Thoma, J. Diez and
 J. Benz, *Angew. Chem., Int. Ed.*, 2011, **1**, 314–318.
- 24 R. Shakya, F. Peng, J. Liu, M. J. Heeg and C. N. Verani,
Inorg. Chem., 2006, **16**, 6263–6268.
- 25 S. S. Hindo, M. Frezza, D. Tomco, M. J. Heeg,
 L. Hryhorczuk, B. R. McGarvey, Q. P. Dou and C. N. Verani,
 40 *Eur. J. Med. Chem.*, 2009, **11**, 4353–4361.
- 26 R. Shakya, C. Imbert, H. P. Hratchian, M. Lanznaster,
 M. J. Heeg, B. R. McGarvey, M. Allard, H. B. Schlegel and
 C. N. Verani, *Dalton Trans.*, 2006, **21**, 2517–2525.
- 27 M. Frezza, C. N. Verani, D. Chen and Q. P. Dou, *Lett. Drug*
Des. Discovery, 2007, **5**, 311–317.
- 28 M. Frezza, S. Hindo, D. Tomco, M. M. Allard, Q. C. Cui,
 M. J. Heeg, D. Chen, Q. P. Dou and C. N. Verani, *Inorg.*
 50 *Chem.*, 2009, **13**, 5928–5937.
- 29 S. Gama, F. Mendes, F. Marques, I. C. Santos,
 M. F. Carvalho, I. Correia, J. C. Pessoa, I. Santos and
 A. Paulo, *J. Inorg. Biochem.*, 2011, **5**, 637–644.
- 30 N. Kordestani, H. A. Rudbari, Z. Fatemina, G. Galjon,
 L. Maes, P. G. Mineo, A. Cordaro, A. Mazaglia, N. Tumanov,
 55 J. Wouters, A. Scala and N. Micale, *Appl. Organomet. Chem.*,
 2021, **35**, e6079.

- 1 31 M. Dehkhodaei, M. Khorshidifard, H. A. Rudbari, M. Sahihi, G. Azimi, N. Habibi, S. Taheri, G. Bruno and R. Azadbakht, *Inorg. Chim. Acta*, 2017, **466**, 48–60.
- 5 32 A. Mukherjee, S. Tothadi and G. R. Desiraju, *Acc. Chem. Res.*, 2014, **8**, 2514–2524.
- 33 K. E. Riley and P. Hobza, *Cryst. Growth Des.*, 2011, **10**, 4272–4278.
- 10 34 Z. Kazemi, H. A. Rudbari, V. Mirkhani, M. Sahihi, M. Moghadam, S. Tangestaninejad, I. Mohammadpoor-Baltork, A. A. Kajani and G. Azimi, *Eur. J. Med. Chem.*, 2017, **135**, 230–240.
- 35 M. Aryaeifar, H. A. Rudbari and G. Bruno, *Polyhedron*, 2018, **155**, 114–128.
- 15 36 J. F. da Silva, K. Shimizu and M. T. Duarte, *CrystEngComm*, 2017, **20**, 2802–2812.
- 37 Y.-X. Sun, R. Z. , L.-F. Zhang, X.-H. Xie and L.-X. Xu, *J. Coord. Chem.*, 2007, **60**, 2607–2619. **Q8**
- 20 38 H. Wang, Y. Lang and S. Wang, *Acta Crystallogr., Sect. E: Struct. Rep. Online*, 2012, **68**, m540.
- 39 R. Kannappan, S. Tanase, I. Mutikainen, U. Turpeinen and J. Reedijk, *Inorg. Chim. Acta*, 2005, **358**, 383–388.
- 40 R. Díaz-Torres and S. Alvarez, *Dalton Trans.*, 2011, **40**, 10742–10750.
- 25 41 N. Kordestani, H. A. Rudbari, A. R. Fernandes, L. R. Raposo, P. V. Baptista, D. Ferreira, G. Bruno, G. Bella, R. Scopelliti, J. Braun, D. E. Herbert and O. Blacque, *ACS Comb. Sci.*, 2020, **22**, 86–89.
- 30 42 K. Czerwińska, B. Machura, S. Kula, S. Krompiec, K. Erfurt, C. Roma-Rodrigues, A. R. Fernandes, L. S. Shul'pina, N. S. Ikonnikov and G. B. Shul'pin, *Dalton Trans.*, 2017, **46**, 9591–9604.
- 35 43 N. Svahn, A. J. Moro, C. Roma-Rodrigues, R. Puttreddy, K. Rissanen, P. V. Baptista, A. R. Fernandes, J. C. Lima and L. Rodriguez, *Chemistry*, 2018, **24**, 14654–14667.
- 44 O. Kepp, L. Galluzzi, M. Lipinski, J. Yuan and G. Kroemer, *Nat. Rev. Drug Discovery*, 2011, **10**, 221–237.
- 40 45 C. Giovannini, P. Matarrese, B. Scazzocchio, M. Sanchez, R. Masella and W. Malorni, *FEBS Lett.*, 2002, **523**, 200–206.
- 46 H. R. Zhang, Y. C. Liu, T. Meng, Q. P. Qin, S. F. Tang, Z. F. Chen, B. Q. Zou, Y.-N. Liua and H. Liang, *Cytotoxicity, MedChemComm*, 2015, **6**, 2224–2231.
- 45 47 T. Meng, S. F. Tang, Q. P. Qin, Y. L. Liang, C. X. Wu, C. Y. Wang, H. T. Yan, J. X. Dong and Y. C. Liu, *MedChemComm*, 2016, **7**, 1802–1811.
- 48 M. Sutradhar, E. Alegria, F. Ferretti, L. R. Raposo, M. F. C. Guedes da Silva, P. V. Baptista, A. R. Fernandes and A. J. L. Pombeiro, *J. Inorg. Biochem.*, 2019, **200**, 110811.
- 49 G. Filomeni, D. De Zio and F. Cecconi, *Cell Death Differ.*, 2015, **22**, 377–388.
- 50 W. Strober, *Curr. Protoc. Immunol.*, 2001, **21**, A.3B.1–A.3B.2.
- 51 E. W. Ainscough, A. M. Brodie, W. A. Denny, G. J. Finlay, S. A. Gothe and J. D. Ranford, *J. Inorg. Biochem.*, 1999, **77**, 125–133.
- 52 W. Y. Lee, P. P. Lee, Y. K. Yan and M. Lau, *Metallomics*, 2010, **2**, 694–705.
- 53 S. Mukherjee, C. Basu, S. Chowdhury, A. P. Chattopadhyay, A. Ghorai, U. Ghosh and H. Stoeckli-Evans, *Inorg. Chim. Acta*, 2010, **363**, 2752–2761.
- 10 54 S. Munira Haidad Ali, Y. K. Yan, P. P. Lee, K. Z. Khong, M. Alam Sk, K. H. Lim, B. Klejevskaja and R. Vilar, *Dalton Trans.*, 2014, **43**, 1449–1459. **Q9**
- 15 55 J. Lakshmipraba, S. Arunachalam, R. V. Solomon, P. Venuvanalingam, A. Riyasdeen, R. Dhivya and M. A. Akbarsha, *J. Biomol. Struct. Dyn.*, 2015, **33**, 877–891.
- 20 56 W. Y. Lee, Y. K. Yan, P. P. Lee, S. J. Tan and K. H. Lim, *Metallomics*, 2012, **4**, 188–196.
- 57 K. Choroba, B. Machura, S. Kula, L. R. Raposo, A. R. Fernandes, R. Kruszynski, K. Erfurt, L. S. Shul'pina, Y. N. Kozlov and G. B. Shul'pin, *Dalton Trans.*, 2019, **48**, 12656–12673.
- 25 58 A. Maron, K. Czerwinska, B. Machura, L. Raposo, C. Roma-Rodrigues, A. R. Fernandes, J. G. Malecki, A. Szlapa-Kula, S. Kula and S. Krompiec, *Dalton Trans.*, 2018, **47**, 6444–6463.
- 30 59 Ma. Zhen, B. Zhang, M. F. C. Guedes da Silva, A. S. Mendo, J. Silva, P. V. Baptista, A. R. Fernandes and A. J. L. Pombeiro, *Dalton Trans.*, 2016, **45**, 5339–5355.
- 60 L. Fialho, D. Araújo, V. D. Alves, C. Roma-Rodrigues, P. V. Baptista, A. R. Fernandes, F. Freitas and M. A. M. Reis, *Int. J. Polym. Mater.*, 2019, 1–10.
- 35 61 *CrysAlis^{Pro}*, *Rigaku Oxford Diffraction, release 1.171.39.46*, 2018.
- 62 A. J. Duisenberg, L. M. Kroon-Batenburg and A. M. Schreurs, *J. Appl. Crystallogr.*, 2003, **2**, 220–229.
- 40 63 R. H. Blessing, *Acta Crystallogr., Sect. A: Found. Crystallogr.*, 1995, **1**, 33–38.
- 64 G. M. Sheldrick, SHELXT - Integrated space-group and crystal-structure determination, *Acta Crystallogr., Sect. A: Found. Adv.*, 2015, **71**, 3–8.
- 45 65 G. M. Sheldrick, SHELXL - Crystal structure refinement, *Acta Crystallogr., Sect. C: Cryst. Struct. Commun.*, 2015, **71**, 3–8.
- 50 66 A. L. Spek, PLATON, *Acta Crystallogr., Sect. D: Biol. Crystallogr.*, 2009, **65**, 148–155.